Interannual Extremes in New Zealand Precipitation Linked to Modes of Southern Hemisphere Climate Variability

CAROLINE C. UMMENHOFER AND MATTHEW H. ENGLAND

Climate and Environmental Dynamics Laboratory, School of Mathematics and Statistics, University of New South Wales, Sydney, Australia

(Manuscript received 4 April 2006, in final form 5 March 2007)

ABSTRACT

Interannual extremes in New Zealand rainfall and their modulation by modes of Southern Hemisphere climate variability are examined in observations and a coupled climate model. North Island extreme dry (wet) years are characterized by locally increased (reduced) sea level pressure (SLP), cold (warm) sea surface temperature (SST) anomalies in the southern Tasman Sea and to the north of the island, and coinciding reduced (enhanced) evaporation upstream of the mean southwesterly airflow. During extreme dry (wet) years in South Island precipitation, an enhanced (reduced) meridional SLP gradient occurs, with circumpolar strengthened (weakened) subpolar westerlies and an easterly (westerly) anomaly in zonal wind in the subtropics. As a result, via Ekman transport, anomalously cold (warm) SST appears under the subpolar westerlies, while anomalies of the opposite sign occur farther north. The phase and magnitude of the resulting SST and evaporation anomalies cannot account for the rainfall extremes over the South Island, suggesting a purely atmospheric mode of variability as the driving factor, in this case the Southern Annular Mode (SAM). New Zealand rainfall variability is predominantly modulated by two Southern Hemisphere climate modes, namely, the El Niño–Southern Oscillation (ENSO) and the SAM, with a latitudinal gradation in influence of the respective phenomena, and a notable interaction with orographic features. While this heterogeneity is apparent both latitudinally and as a result of orographic effects, climate modes can force local rainfall anomalies with considerable variations across both islands. North Island precipitation is for the most part regulated by both local air–sea heat fluxes and circulation changes associated with the tropical ENSO mode. In contrast, for the South Island the influence of the large-scale general atmospheric circulation dominates, especially via the strength and position of the subpolar westerlies, which are modulated by the extratropical SAM.

1. Introduction

Located in the Southern Hemisphere in the path of the subpolar westerlies and relatively remote from other landmasses, atmospheric circulation dominates New Zealand's weather and climate. Rainfall over New Zealand is influenced by the interaction of the orography of an essentially mountainous country with the atmospheric circulation (Salinger et al. 1995; Salinger and Mullan 1999). Situated in the midlatitudes, the country experiences tropical and subtropical influences from the Pacific as well as high-latitude effects from the southern Pacific and Southern Oceans. Tropical convection in the equatorial Pacific impacts on large-scale Southern Hemisphere circulation and therefore New Zealand climate, especially during extreme years of the El Niño–Southern Oscillation (ENSO; Kidson and Renwick 2002). Similarly, the strength and position of the subtropical jet, the subtropical high-pressure belt, and the subpolar westerlies influence New Zealand's climate (Clare et al. 2002), as do extratropical storm tracks (Simmonds and Keay 2000; Keable et al. 2002). Interannual variability in New Zealand climate has been linked to a number of large-scale Southern Hemisphere climate modes, including the Antarctic Circumpolar Wave (ACW; White and Cherry 1999); ENSO (Kidson and Renwick 2002; Carleton 2003); the high-latitude mode, more commonly termed the Southern Annular Mode (SAM; Clare et al. 2002); and the Interdecadal Pacific Oscillation (IPO; Salinger et al. 2001).

The complex interactions between tropical/subtropical and high-latitude influences, along with the synop-

Corresponding author address: Caroline C. Ummenhofer, Climate and Environmental Dynamics Laboratory, School of Mathematics and Statistics, University of New South Wales, Sydney, NSW 2052, Australia.
E-mail: c.ummenhofer@unsw.edu.au

DOI: 10.1175/2007JCLI1430.1

tic nature of atmospheric circulation at midlatitudes, make New Zealand's climate difficult to predict over seasonal to interannual time scales. This is exacerbated by the sparse data coverage over the Southern Hemisphere prior to 1970, which precludes analysis of a long, high-quality data record. In this study, we combine observations and reanalysis data with output from a 200-yr unforced natural variability run of a coupled climate model, an approach not used for the region to date, to investigate factors influencing interannual variations in New Zealand rainfall. In a future study, we will separately investigate long-term trends in New Zealand rainfall during the second half of the twentieth century and their relation to trends in Southern Hemisphere climate modes. For the present study, our focus remains on the interannual time scale.

Previous work on the New Zealand climate concentrates on the use of station (Madden et al. 1999; Salinger and Mullan 1999; Salinger and Griffiths 2001) and reanalysis data (Mullan 1998). To our knowledge only Renwick et al. (1998) use model data, in their case the Commonwealth and Scientific Industrial Research Organisation (CSIRO) Division of Atmospheric Research Limited Area Model (DARLAM), nested in the CSIRO Mark 2 model to examine spatial properties of precipitation and surface temperature across New Zealand. Their results were highly dependent on model resolution, especially the frequency of extreme events, and the authors identify deficiencies linked to an overly vigorous zonal flow in the model. In the present study, we combine direct observations, reanalysis data, and output from coupled climate models to explore New Zealand's interannual rainfall variability.

The high proportion of mountainous regions over the country's surface area, especially on the South Island, leads to considerable heterogeneity in climate fields over short distances (e.g., rainfall; Fig. 1). Nonetheless, attempts have been made to explain local characteristics in New Zealand's climate as a result of the large-scale general circulation and its variability. For example, Mullan (1998) investigates lag associations between reanalyzed sea surface temperature (SST) and New Zealand station data of temperature, precipitation, and mean sea level pressure (MSLP) for the second half of the twentieth century. On seasonal time scales, he finds several lag relationships, some of which relate to ENSO and Indian Ocean SST, that suggest the SST surrounding New Zealand responds to variability in the general circulation. Further connections to ENSO are described by Fitzharris et al. (1997), relating positive (negative) New Zealand glacial mass balance to El Niño (La Niña) events. In addition, Salinger et al. (2001) investigate the effect of the IPO on the South

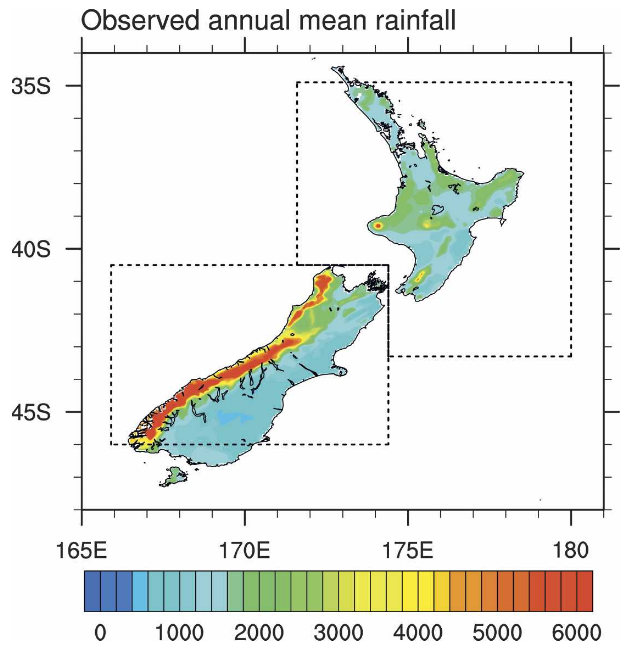

FIG. 1. Annual mean precipitation map for New Zealand for the period 1960–2004 (in mm yr^{-1}). The thin dashed boxes indicate the areas over which a spatial average was employed to calculate the model precipitation time series for the North and South Island, respectively, in the NCAR CCSM2 unforced natural variability simulations.

Pacific climate during the period 1931–98, finding a modulating influence of the IPO on ENSO teleconnection patterns around Australia and New Zealand. By modulating the South Pacific Convergence Zone (SPCZ), the IPO is found to favor stronger ENSO teleconnections in the northeast of New Zealand during its positive phase, with El Niño (La Niña) periods being drier (wetter) since 1977. In contrast to other studies, White and Cherry (1999) relate variations in New Zealand temperature and precipitation directly to SST anomalies associated with the ACW. They find empirical orthogonal function (EOF) patterns of autumn–winter station data over New Zealand for the period 1982–95 to vary in phase with SST anomalies. They argue that ACW-driven anomalies in SST and surface winds around New Zealand set up anomalous low-level wind convergence and cyclonicity during years of increased autumn–winter precipitation. However, their study period 1982–95 is very short and will be extended in the present analysis and combined with output from a multicentury coupled climate model.

Apart from the above study by White and Cherry (1999), only Clare et al. (2002) have made a link between New Zealand rainfall and high-latitude climate modes. Clare et al. (2002) found a modulating influence of the SAM on end-of-summer snowlines in the Southern Alps, New Zealand. They suggest that the SAM affects snowlines via weakened (strengthened) zonal flow carrying a reduced (increased) number of depressions over the New Zealand region during its low (high) phases. SAM influences on rainfall in other midlatitude regions have been shown previously: for example, for southwest Western Australia by shifting the position of the maximum temperature gradient and modulating baroclinic instability (Cai et al. 2005); across the Australian continent (Meneghini et al. 2006); for South America via changes to the upper-level atmospheric circulation and moisture convergence (Silvestri and Vera 2003); and for South Africa via shifts in the position of the subtropical jet and associated moisture flux (Reason and Rouault 2005).

This is the first study to investigate the impact of the SAM on New Zealand's interannual precipitation. In addition, we assess the respective influence of two prominent Southern Hemisphere climate modes (SAM and ENSO) on New Zealand rainfall variability, along with the associated atmospheric circulation, by using an extended simulation from a coupled climate model in combination with available observations and reanalysis data. High-quality observations in the mid- to high latitudes of the Southern Hemisphere are sparse, especially over the oceans, and data coverage has only increased in recent years. We therefore have no high-quality extended data record for our analyses, which results in only a relatively small number of anomalously dry and wet years employed in composites. Using output from a 200-yr unforced natural variability coupled climate model run provides an additional means of assessing modes of New Zealand rainfall variability. In particular, the model time series includes approximately 30 anomalously dry and wet years in the composites, which allows an independent assessment of the robustness of the reanalysis findings. This is an approach used successfully in previous studies for other regions of the Southern Hemisphere (e.g., England et al. 2006). Of particular interest in this study are the relative roles of the SAM and ENSO in controlling interannual New Zealand rainfall variability via changes to the large-scale ocean and/or atmospheric circulation. This will be investigated in more detail with composites during extreme phases of ENSO and the SAM, complementing the approach of compositing anomalously high–low rainfall years across New Zealand.

The rest of the paper is outlined as follows: section 2 describes the datasets and the model, as well as the methods and techniques used. Section 3 details precipitation observations across New Zealand and composites of reanalysis and model data during years of anomalously high and low precipitation. In section 4, relationships between New Zealand precipitation and Southern Hemisphere climate patterns are investigated in more detail. Section 5 summarizes the results of the study.

2. Data and data analysis

a. Observational data

The observational New Zealand precipitation data analyzed in this study is taken from the National Institute of Water and Atmospheric Research (NIWA) Climate Database. It comprises daily New Zealand station data that has been interpolated to give a gridded dataset with a 0.05° latitude/longitude (approximately 5 km) resolution for the entire country. The daily gridded precipitation data is converted to monthly and annual rainfall totals for the time period 1960–2004.

The data for regional and large-scale analysis of atmospheric parameters, such as sea level pressure (SLP), surface winds, and surface heat and moisture fluxes, among others, is part of the National Centers for Environmental Prediction (NCEP)–National Center for Atmospheric Research (NCAR) reanalysis project (Kalnay et al. 1996; Kistler et al. 2001). The NCEP–NCAR reanalysis assimilates land- and ocean-based observations and satellite measurements and, by employing a global spectral model, generates a dataset with global coverage for a wide set of climatic parameters with a horizontal resolution of T62 (approximately 2° latitude/longitude) going back to 1948. However, we only analyze monthly data for the same time period as the rainfall observations, that is, 1960–2004. Problems regarding data coverage and quality in the high latitudes of the Southern Hemisphere prior to 1979 have been documented (Hines et al. 2000; Marshall and Harangozo 2000; Kistler et al. 2001; Marshall 2002, 2003; Renwick 2004). However, on seasonal to interannual time scales the NCEP–NCAR reanalysis fields are in overall good agreement with observations (Hines et al. 2000; Kistler et al. 2001). In addition, for comparison, the analyses are repeated with the 40-yr European Centre for Medium-Range Weather Forecasts (ECMWF) Re-Analysis (ERA-40) for the period 1960–2001 (Uppala et al. 2005). Monthly SST is employed for 1960–2002 from the extended reconstructed dataset developed by the National Oceanic and Atmospheric Administration (NOAA) with a 2° horizontal resolution (Smith and Reynolds 2003, 2004). All analyses are performed on annually averaged data.

b. Climate model

Apart from analyzing the above climatologies, we also examine the mechanisms controlling New Zealand rainfall within a 200-yr unforced natural variability run of the NCAR Community Climate System Model, version 2 (CCSM2; Kiehl and Gent 2004). The atmospheric component of CCSM2 uses a spectral dynamical core, a T42 horizontal resolution (approximately 2.8° latitude–longitude), and 26 vertical levels. The ocean component is based on the Parallel Ocean Program (POP) and its grid uses spherical coordinates in the Southern Hemisphere. Its horizontal resolution is constant in longitude (1.125°), but varies with latitude from 0.27° in the Tropics to 0.5° at mid- to high latitudes. In the vertical there are 40 geopotential levels at 10-m resolution from the surface down to 50 m, and increasing toward 250-m intervals in the abyssal ocean. For further information on the CCSM2 model and its components see Kiehl and Gent (2004) and Boville and Gent (1998). Key model analyses are repeated with the latest version of NCAR's coupled climate model, CCSM3, details of which can be found in Collins et al. (2006). The mean annual model rainfall for the New Zealand region is compared to the Climate Prediction Center (CPC) Merged Analysis of Precipitation (CMAP; Xie and Arkin 1996) climatology for the period 1979–2004. The CMAP dataset has an approximately 2.5° latitude/longitude resolution and combines satellite measurements, gauge-based analyses from the Global Precipitation Climatology Center, and operational forecast data from ECMWF.

c. *Data analysis and statistical methods*

Given the relatively large latitudinal extent of New Zealand, we have stratified our analyses separately for the North and South Islands. For each island, time series are calculated of the monthly and annual mean precipitation as a spatial area average. For the observed annual rainfall records, the least squares linear trend (-8.13 mm yr^{-1} and -0.03 mm yr^{-1} for the North and South Islands, respectively) is removed, along with the mean, to give a detrended time series of anomalies. This time series forms the basis for our analysis of anomalously dry and wet years in New Zealand rainfall.

Because of the coarser resolution of the coupled CCSM2 model, two slightly larger regions are formed for the South and North Islands, respectively (see boxes in Fig. 1). The first region (40.5°–46.0°S, 165.9°–174.4°E, consisting of 3×4 grid boxes) coincides with the South Island of New Zealand and the other one (34.9°–43.3°S, 171.6°–180.0°E, consisting of 4×4 grid boxes, though the southwestern most grid box overlapping the South Island has been excluded) with the North Island. Though not all grid boxes used to form the model rainfall time series for the two islands are exclusively land points, most are covered by at least some fraction of land. Only a negligible linear trend is discernible for the model precipitation time series for both regions, so the time series are not detrended. This contrasts with the observations, particularly for the North Island, where a clear multidecadal decline is apparent. However, with the model data resulting from an unforced natural variability simulation, we expect and are reassured by the absence of any long-term trends.

For both observations and model, composites of anomalies are formed for years of extreme precipitation from the anomalous precipitation time series for the two islands of New Zealand. Years exceeding the cutoff value of ± 1 standard deviation are considered wet and dry years, respectively. While we stratify our analyses into North and South Island rainfall, we do not propose a priori that one island will uniformly respond to any given mode of climate variability, nor that a given climate mode projects onto each island distinctly. Indeed, we will see later that dry (wet) years for each island are also associated with significant regions of below- (above-) average rainfall for the adjacent New Zealand island. Throughout the study, we use a two-tailed t test to determine the significance of the spatial composite fields. This test estimates the statistical significance by which the mean of the composite anomalies for extreme years is distinguishable from zero at each grid point.

Extreme year composites of anomalous New Zealand rainfall observations are compared to patterns associated with ENSO and the SAM. The years taken as El Niño and La Niña years are taken to be those defined by Meyers et al. (2007) for the period 1960–99. All 8 El Niño years occurring during this period were defined as certain, while this was true for only 4 out of 10 La Niña years. However, as separate analyses for certain and debatable La Niña years gave very similar results, composites for all 10 La Niña events are presented here. There is no general consensus on ENSO years after 1999, but increased Niño-3 temperatures occurred during 2002 (Gary Meyers 2006, personal communication). Thus, the year 2002 was included as an additional El Niño year. The monthly SAM index used here (Todd Mitchell 2006, personal communication) is the principal component (PC) time series of the leading EOF of NCEP–NCAR reanalyzed SLP anomalies south of 20°S, standardized with respect to the period 1979–2004. The index is highly correlated with that of Thompson and Wallace (2000), which is based on 850-hPa geopotential height, for the period in common, that is, for 1958–97 (Todd Mitchell 2006, personal communication; additional information available online at http://www.jisao.washington.edu/aao/slp). A SAM index based on NCEP–NCAR reanalyzed

SLP has been used previously (e.g., Gong and Wang 1999) and Jones and Widmann (2003) further discuss its validity. As described above, the monthly SAM index is converted to annual values and detrended before determining extreme years of the SAM, that is, those exceeding ± 1 standard deviation from the detrended mean. This results in 8 extreme positive and 8 extreme negative SAM years. It is noted that we also analyzed composite properties derived from monthly extremes in the SAM, and obtained qualitatively similar results, as would be expected when the SAM directly controls New Zealand rainfall via internal atmospheric variability. For the model, ENSO and SAM years were determined similarly as those exceeding ± 1 standard deviation in the time series. The ENSO years were derived from an annual Niño-3.4 index calculated from SST anomalies for the region 5°N–5°S, 120°–170°W. The SAM years were calculated from the annual PC time series of the first leading EOF performed on SLP anomalies south of 20°S. Both time series were detrended and normalized by dividing by their standard deviation.

3. Results

a. Precipitation observations

The NIWA precipitation observations show high spatial variability in rainfall over New Zealand. Precipitation patterns for the North and South Islands are distinctly different both in overall rainfall amounts and their seasonal distribution (Figs. 1 and 2). The high-rainfall region along the mountainous west coast of the South Island is dominant throughout the year with mean annual values in excess of 6000 mm yr^{-1} (Fig. 1). The eastern part of the South Island receives considerably less rainfall at an average of about 600–1500 mm yr^{-1}. The North Island does not show such a clear gradation in either the east–west or north–south sense. Rainfall there is mostly in the range of 900 and 3000 mm yr^{-1}, with a few highly localized high-rainfall regions in excess of 4000 mm yr^{-1}. For the period 1960–2004, the area-averaged annual mean rainfall for the North Island (1600 mm yr^{-1}) is comparatively lower than the South Island (2085 mm yr^{-1}). A prominent trend (-8.13 mm yr^{-1}) of overall decreasing precipitation is observed over the North Island for the period 1960–2004 (removed in Fig. 2b). In contrast, only a negligible trend (-0.03 mm yr^{-1}) appears in the area-integrated South Island precipitation record. Anomalously dry and wet years for both the South and North Islands are indicated in Figs. 2a,b as those years exceeding one standard deviation from the annual mean. For the period 1960–2004, only very few extreme years are shared between the two islands, namely, 1961 (dry), 1968 (wet), and 1995 (wet) (see also Table 1). One year, 1983, appears as an extreme year of opposite sign; being anomalously dry for the North Island and wet for the South Island. Extreme years for the North (South) Island include 7 (8) dry and 8 (10) wet years during the length of the record investigated (Table 1).

The characteristics of the two islands also differ in their respective seasonal cycles (Figs. 2c,d): the South Island precipitation occurs more or less uniformly throughout the year, while the North Island shows slightly increased monthly rainfall during austral winter (May–October). Precipitation in anomalous high and low rainfall years for the South Island deviates mostly from the mean rainfall distribution during early austral spring (August–October), and less so for autumn (March–May; Fig. 2c). In contrast, for the North Island, the seasonal rainfall distribution during dry and wet years mirrors the average seasonal cycle closely (Fig. 2d). The distribution of rainfall is not significantly different from a uniform value (at 90% confidence level) for both the North and South Island. This allows us to concentrate our analyses on the annual mean fields.

A power spectral density analysis is performed for both observed and model annual precipitation time series as follows: the mean and least squares linear trend are removed, smoothing is applied, and 10% of the data is tapered. A theoretical "white noise" spectrum is calculated to determine frequencies dominant at the 90% significance level. The power spectral density analysis reveals no high-frequency variability to be significant for either of the two islands (Figs. 2e,f), confirming that subannual variability is weak compared to year-to-year fluctuations. This lends further support to an analysis of interannual—not intra-annual—rainfall variability over New Zealand. At longer time scales, broad peaks occur at approximately 4 yr for the South Island and at approximately 4.5 and 3 yr for the North Island.

In addition to the temporal variability, the spatial variation of rainfall across New Zealand during extreme years for both islands is presented in Fig. 3. It shows extreme years for both the North and South Island to be consistently dry/wet for the entire island. During dry years in the South Island, the entire southern island and southern regions of the North Island receive 100–400 mm yr^{-1} below normal precipitation (Fig. 3a). Wetter conditions in excess of 200 mm yr^{-1} only prevail along the very northern and eastern coast of the North Island. South Island wet years are characterized by wetter conditions for the entire western and southern regions of the two islands, with negligible changes along the eastern coastlines (Fig. 3b). For the North Island dry (wet) years, anomalously low (high)

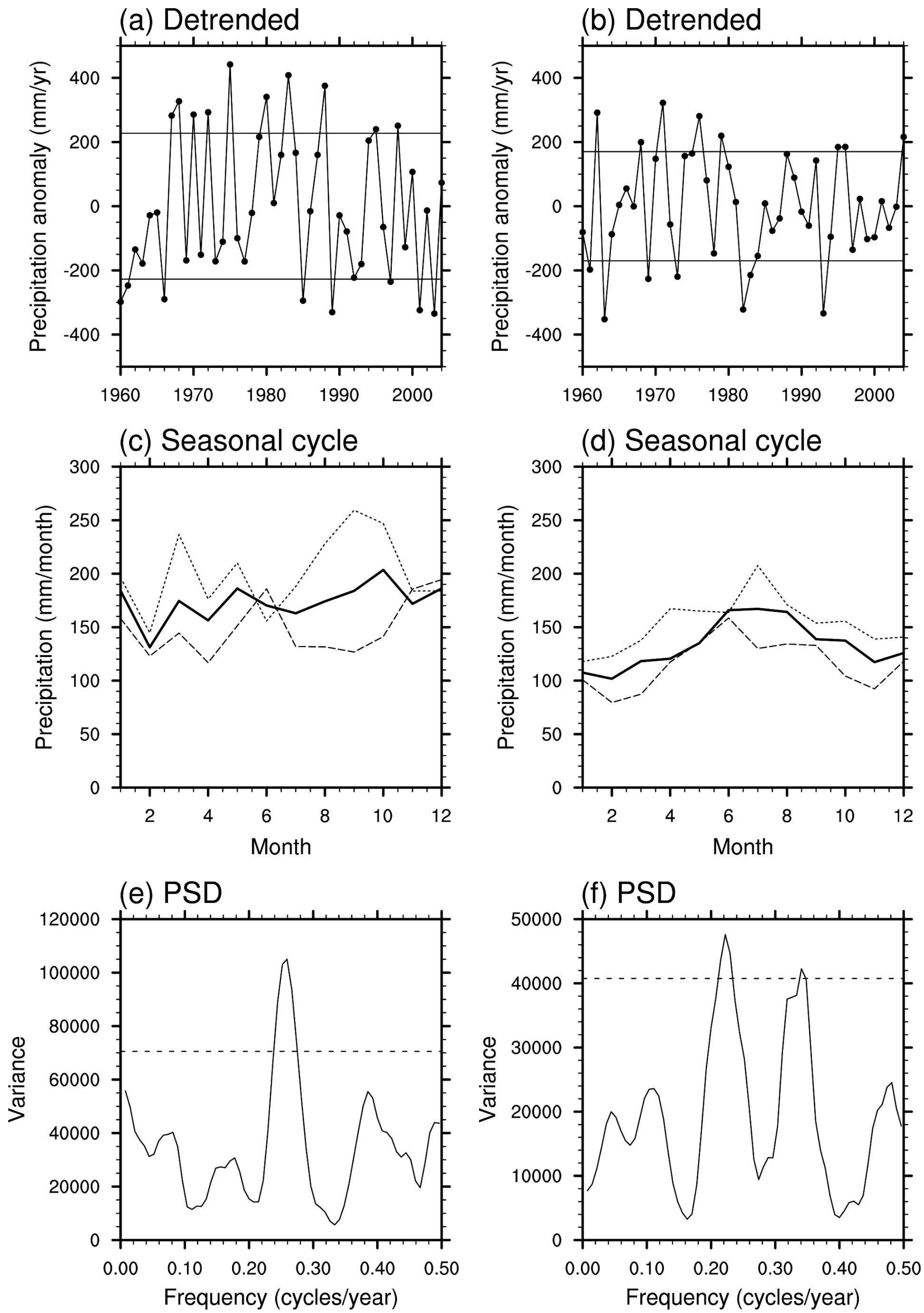

Fig. 2. Characteristics of observed precipitation time series for the (left) South Island and (right) North Island: (a), (b) detrended annual anomalies in mm yr^{-1} with horizontal lines indicating cutoff values for extreme years; (c), (d) seasonal cycle (mm $month^{-1}$) averaged over all years (solid line) or only dry (dashed) and wet (dotted) years, respectively; and (e), (f) power spectral density with theoretical white noise spectrum at the 90% confidence level (dashed horizontal line).

TABLE 1. Years of anomalous precipitation for the South and North Islands of New Zealand for the period 1960–2004 (determined as those years exceeding the cutoff value of ±1 std dev). Here ±EN indicates El Niño and La Niña years (as defined by Meyers et al. 2007) and ±SAM indicates positive and negative years for the SAM.

Island	Dry	Wet
South Island	1960	1967
	1961	1968
	1966	1970
	1985 (+SAM)	1972 (+EN, −SAM)
	1989 (+SAM)	1975 (−EN)
	1997 (+EN)	1980 (−SAM)
	2001	1983
	2003 (−SAM)	1988 (−EN)
		1995
		1998 (+SAM)
North Island	1961	1962 (+SAM)
	1963 (+EN)	1968
	1969	1971
	1973 (−EN, +SAM)	1976
	1982 (+EN)	1979 (+SAM)
	1983	1995
	1993 (+SAM)	1996
		2004

rainfall in excess of 200 mm yr^{-1} occurs for the entire North Island and northern and eastern regions of the South Island (Figs. 3c,d). In contrast, along the west coast of the South Island dry conditions dominate in both dry and wet North Island years. Overall though, the anomalous patterns of rainfall indicate "all island" responses for both dry and wet years for each island. That is, each island exhibits a coherent below- and above-average rainfall pattern, on average, during years of anomalous total island rainfall.

b. *Climate during New Zealand extreme years*

1) REANALYSIS FIELDS

Composites of various atmospheric NCEP–NCAR reanalyzed fields are investigated for anomalous rainfall years in the two New Zealand islands during the period 1960–2004 (Figs. 4 and 5). During South Island dry (wet) years, an intensification of the meridional SLP gradient occurs (Figs. 4a,b). Significant positive (negative) anomalies (in excess of ±1.5 hPa) appear across a latitude band 30°–60°S from the subtropical Indian Ocean to the middle of the Pacific basin. Composites for anomalous rainfall years over the North Island show less of a circumpolar pattern in SLP anomalies (cf. Figs. 4a,b to Figs. 5a,b), instead exhibiting a dipole pattern. One significantly positive (negative) pole during dry (wet) years occurs across New Zealand and eastern Australia, and the other negative (positive) pole is located to the east of New Zealand across the subtropical south Pacific gyre. The circumpolar nature of the SLP anomalies, especially for the South Island anomalously dry and wet years, is reminiscent of the pattern widely associated with the SAM (e.g., Gong and Wang 1999; Thompson and Wallace 2000).

The anomalous SLP fields force, according to geostrophy, changed zonal wind fields of a similar circumpolar nature for South Island anomalous rainfall years (Figs. 4c,d). A strengthening (weakening) of the subpolar westerlies is observed during years of dry (wet) South Island extremes at 50°–70°S, while a weakening (strengthening) of a similar magnitude (up to ±0.8 m s^{-1}) is seen to the north for the latitude band 30°–50°S. These changes in zonal wind are again characteristic of the increased MSLP gradient between mid- and high latitudes linked to the SAM (Thompson and Wallace 2000; Hall and Visbeck 2002). Associations between the SAM and extratropical storm tracks, as described by Rao et al. (2003), and observed and projected poleward shifts in the position of the storm tracks under a more positive SAM phase (Fyfe 2003; Yin 2005) could account for the reduced rainfall across the South Island during dry years. Dry (wet) years also coincide with more southerly (northerly) wind anomalies across New Zealand, and especially over a region to the northeast of the country (Figs. 4c,d), affecting local moisture transport onto the islands. Regions of positive (negative) westerly anomalies across New Zealand during dry (wet) North Island years stretch in a southwest–northeast direction from 120°E–150°W and 30°–70°S (Figs. 5c,d). These anomalies are followed further north by a similar band of easterly (westerly) wind anomalies across Tasmania and eastern Australia. The New Zealand region and adjacent ocean also experiences southerly (northerly) wind anomalies during dry (wet) North Island years (Figs. 5c,d), varying local moisture fluxes. Composite anomalies of ERA-40 SLP and winds (figures not shown) indicate qualitatively very similar results, though the level of significance differs slightly and the circumpolar character of the anomalies is marginally more pronounced in ERA-40.

Localized changes in moisture flux due to local wind anomalies seem to be more important for the North Island of New Zealand. Humidity is generally reduced (increased) during dry (wet) years in northern New Zealand over the land itself and the surrounding ocean regions (figure not shown) because of reduced (increased) latent heat flux from the ocean in the immediate vicinity of the island (figure not shown). This, along with the anomalous offshore (onshore) local winds, contributes to dry (wet) conditions over the North Island. In contrast, anomalous composite fields

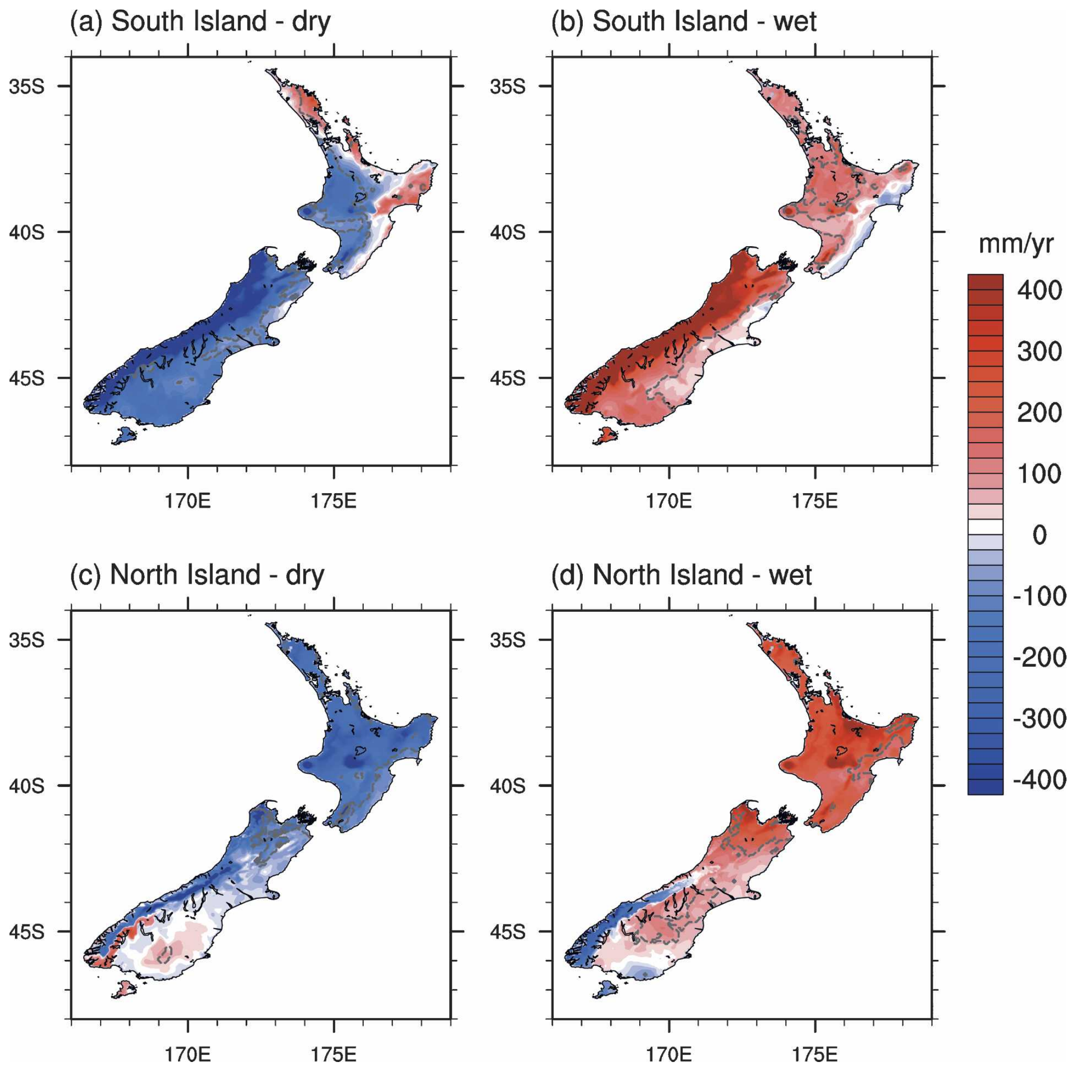

FIG. 3. Composites of observed precipitation anomalies for (a), (b) South Island and (c), (d) North Island for anomalously (left) dry and (right) wet rainfall years. Gray dashed lines indicate significant anomalies at the 90% confidence level as estimated by a two-tailed *t* test.

of humidity and latent and sensible heat fluxes during anomalously dry and wet South Island years show no consistent patterns to explain the rainfall anomalies. This issue will be revisited below for the model simulations.

Anomalous composite fields of SST indicate warm (cold), though mainly insignificant, anomalies (up to $\pm 0.3°C$) around New Zealand and the Tasman Sea during dry (wet) South Island years (Figs. 4e,f). Smaller anomalies of the opposite sign—that is, cold (warm) during dry (wet) years—occur to the north of New Zealand and across the Coral Sea. The small area of statistically significant SST anomalies in the composites is in part symptomatic of the short observational record (1960–2002), resulting in few extreme years (7–10 anomalously dry/wet years). This signal has to then be compared in significance to the natural year-to-year variability in SST (Fig. 6c). So, small areas of significance do not necessarily imply that rainfall over the two islands is largely atmospheric driven. To resolve this issue we investigate latent heat fluxes and employ output from a 200-yr natural variability run of the CCSM2 model, providing approximately 30 anomalously dry and wet years (see next section). As seen in composites of latent heat fluxes (figure not shown) these SST anomalies are indeed not significantly contributing to the observed rainfall anomalies via changes in the evaporation. The SST anomalies are rather symptomatic of the changed general atmospheric circulation during dry (wet) South Island years: the poleward (equa-

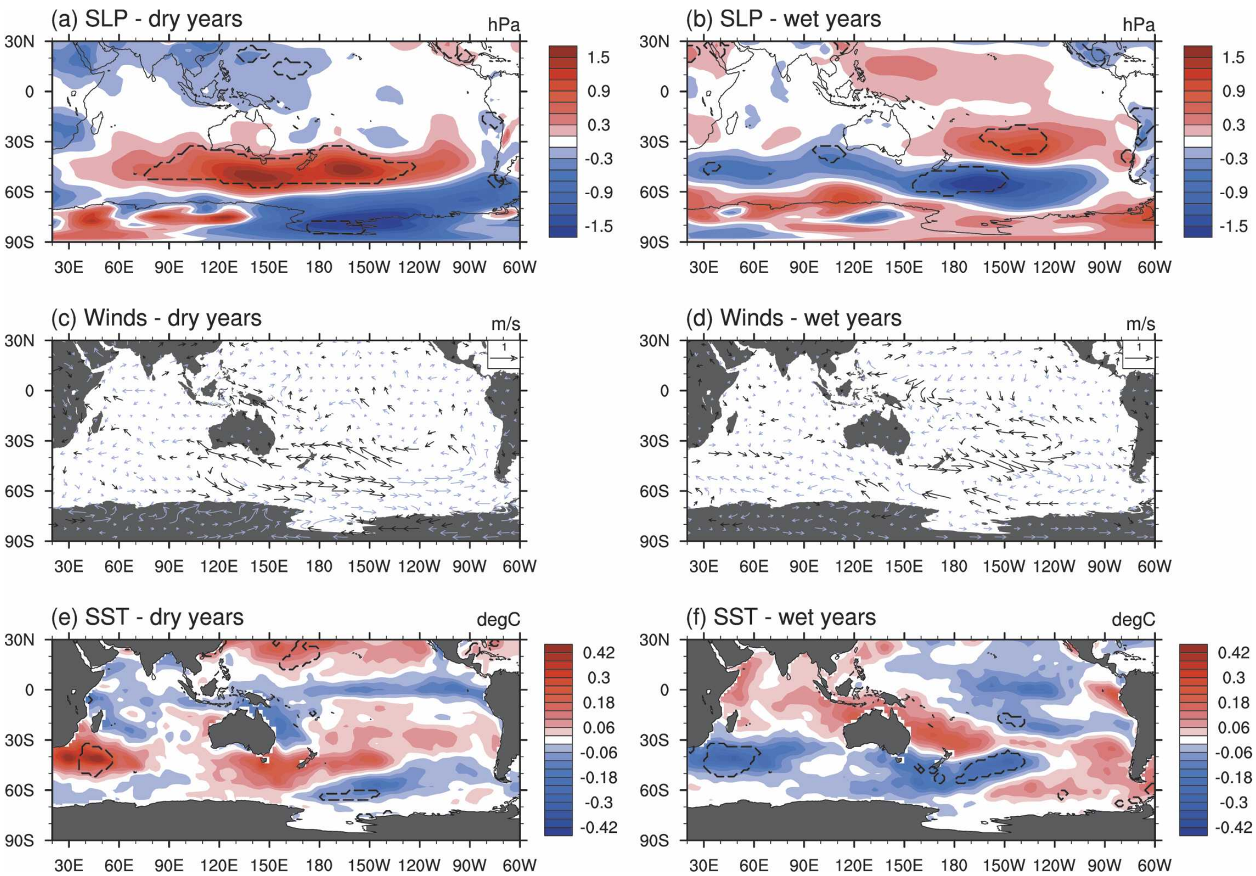

FIG. 4. Composite anomalies in observed (a), (b) SLP, (c), (d) winds, and (e), (f) SST for the South Island for anomalously (left) dry and (right) wet rainfall years. Dashed lines and black vectors indicate significant anomalies at the 90% confidence level as estimated by a two-tailed t test.

torward) shift and strengthening (weakening) of the subpolar westerlies south of 50°S and easterly (westerly) anomaly to the north for the latitude band 30°–50°S lead to anomalously warm (cold) SST for the latitude band 40°–60°S (Figs. 4e,f) likely due to anomalous wind-driven Ekman transport. In contrast, during North Island dry (wet) years, cold (warm) anomalies around New Zealand dominate, with a small area of opposite sign along the east Australian coast (Figs. 5e,f). These SST anomalies can account for the anomalous latent heat fluxes described earlier and thereby contribute via reduced (increased) evaporation and changed local wind fields to dry (wet) conditions for northern New Zealand. These results suggest that northern New Zealand climate is influenced by local air–sea heat fluxes. In contrast, rainfall anomalies over the South Island are controlled by the large-scale general circulation. In addition, a prominent, though nonsignificant, El Niño- (La Niña-) type warming (cooling) in excess of ±0.4°C is observed in the eastern tropical Pacific Ocean during dry (wet) North Island years, suggestive of a possible ENSO influence on the northern island's precipitation.

2) MODEL

To assess the suitability of the CCSM2 model for this study, we compare the model variability in SST and SLP in the region to observations (Fig. 6). This simple analysis helps reveal the relative intensity and patterns of ENSO and SAM in comparison to the observations. The standard deviation of SLP shows a latitudinal gradient in the observations with higher variability (in excess of 1.8 hPa) in the high latitudes south of 60°S, diminishing to 1–1.5 hPa in the midlatitudes and less in the Tropics (Fig. 6a). The broad features of the latitudinal gradient of the SLP standard deviation is reproduced well in the model (Fig. 6b). However, over New Zealand and the Tasman Sea, the model shows slightly higher variability than the observations, while a band of lower variability in the model extends across the Indian Ocean sector of the Southern Ocean between 50°–60°S.

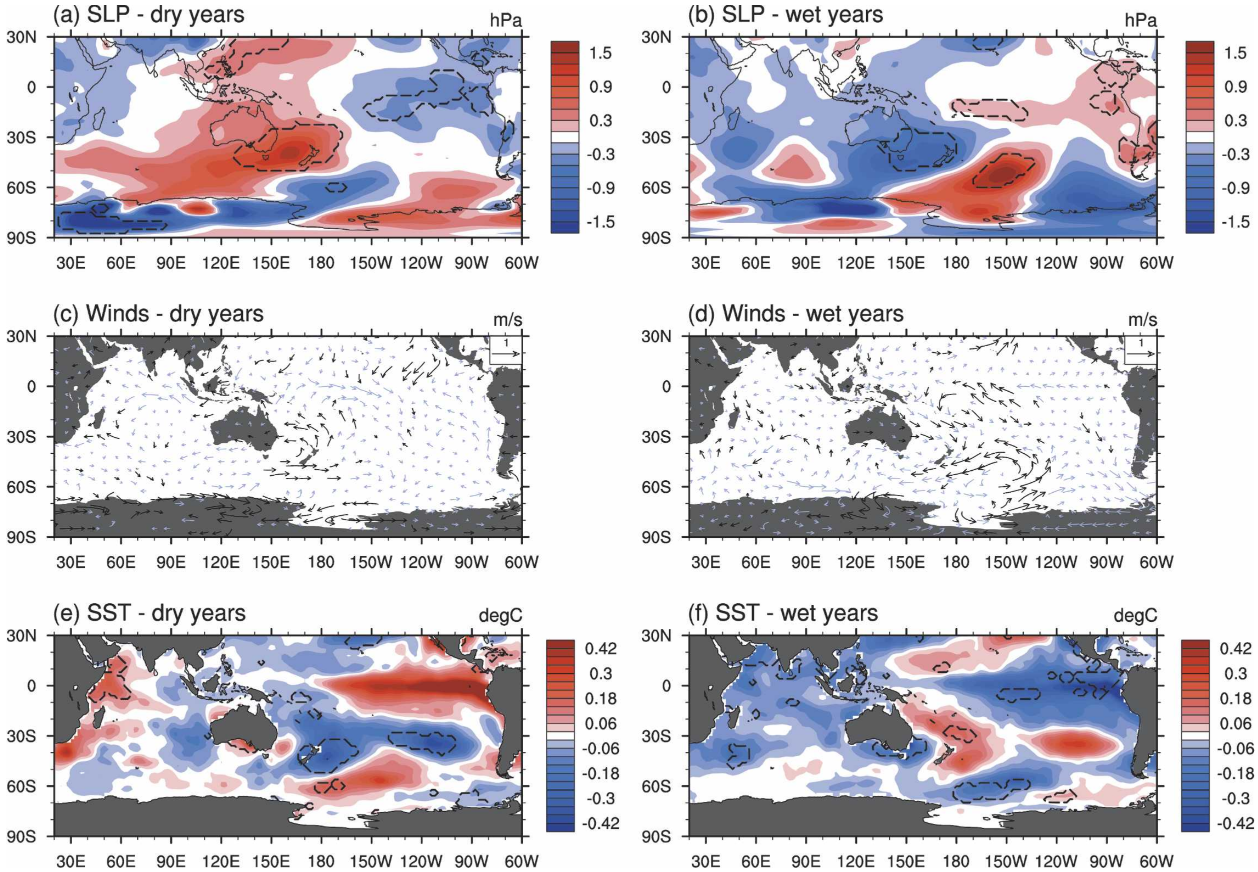

FIG. 5. Same as Fig. 4, but for the North Island.

Sen Gupta and England (2006) found that the SAM projects too strongly onto SST, but the effect on winds (especially zonal flow) is well captured in the model. They suggest that the disagreement in the SST response to the SAM forcing between the model and observations is due in part to the short observational record and sparse data coverage in the high latitudes of the Southern Hemisphere. The SST variability in the equatorial Pacific Ocean in the model and observed differ in their magnitude, with the observed showing greater variance in the eastern equatorial Pacific, and lower variance in the western Pacific warm pool region compared to the model (Figs. 6c,d). The extension of the model's ENSO pattern too far west in the Pacific Ocean (Fig. 6d) was described in detail by Kiehl and Gent (2004) and Collins et al. (2006). The ENSO in the model also has a dominant frequency of around 2–3 yr (e.g., Kiehl and Gent 2004; Collins et al. 2006), which compares with the longer period of 3–5 (Collins et al. 2006), 3–7 (Kiehl and Gent 2004), or 3–8 (Zelle et al. 2005) years in the observed. However, for the scope of this study, reasonable agreement between the model and observations is found on interannual time scales for the spatial and temporal variability of the SAM and ENSO, as shown previously by Sen Gupta and England (2006) and Hack et al. (2006), respectively. To further corroborate this we repeated key analyses with output from the CCSM3 model and ERA-40 and found qualitatively similar results and conclusions.

Comparison of the annual mean CCSM2 model precipitation with the CMAP climatology shows that the model reproduces the large-scale features in rainfall over the southwestern Pacific region reasonably well (Fig. 7). The high-rainfall region over the equatorial western Pacific is captured, as is the low-rainfall domain over the interior of the Australian continent. The extent and position of the Intertropical Convergence Zone (ITCZ) and SPCZ in the model show some deficiencies. Details of the model's performance in the ITCZ and SPCZ in the western Pacific region can be found in Kiehl and Gent (2004), Collins et al. (2006), and Hack et al. (2006). Biases in the characteristics of the Pacific ITCZ are common to many coupled climate models (Kiehl and Gent 2004; Zhang and Wang 2006), particularly those without flux adjustments (Meehl et al. 2001). In CCSM3 as in previous versions, a persis-

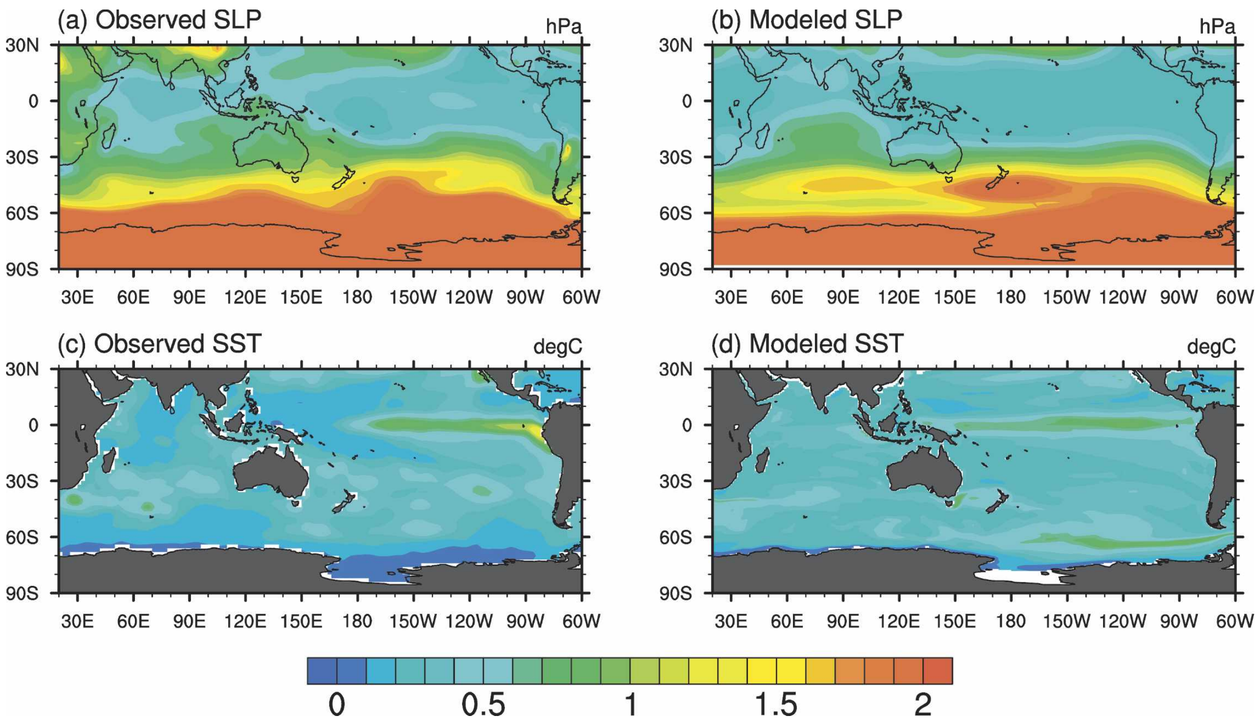

FIG. 6. Standard deviation in (left) observations and (right) the CCSM2 model of (a), (b) annual mean SLP (hPa) and (c), (d) annual mean SST (°C). The observations cover the period 1960–2004 for SLP and 1960–2002 for SST; the model output is for 200 yr.

tent bias exists toward a double ITCZ and too strong a SPCZ extending too far to the southeast into the central Pacific Ocean (Collins et al. 2006; Hack et al. 2006). However, Hack et al. (2006) conclude that the hydrological cycle in the atmospheric component of CCSM3 more closely resembles observations compared to previous model versions and captures the major features of the water cycle well on seasonal to interannual time scales, also as associated with ENSO. After comparing our results for both the CCSM2 and CCSM3 models, we conclude that the precipitation representation in the southern Pacific is sufficiently good on interannual time scales. Nonetheless, we have carefully assessed our results for CCSM2 and compared them to both reanalyses and observations over the New Zealand region, as well as CCSM3 results. Over New Zealand, the very localized region of enhanced precipitation along the mountainous west coast of the South Island in CMAP is apparent in the model as well, though lower in magnitude and extending over a wider area. The difference in observed rainfall between the North and South Islands are also reproduced in the model (Fig. 7b), even if the absolute rainfall amounts are reduced for both islands compared to the observations.

A detailed analysis of the time series of the 200 yr of New Zealand precipitation fluctuations (Fig. 8) also shows the model captures two different regimes over the two New Zealand islands. Though the model rainfall anomalies for the two islands are smaller, they are of similar magnitude in relation to the annual precipitation as in the observed (i.e., 13%–15% of the mean annual precipitation). The annual mean precipitation for the South and North Island is 1150 mm yr^{-1} and 1060 mm yr^{-1}, respectively. Following the method described above, years with anomalous high and low precipitation are chosen as those exceeding ± 1 standard deviation of the mean, resulting in 30 (31) anomalously low (high) rainfall years for the South and 32 (30) anomalously dry (wet) years for the North Island (Figs. 8a,b). The relative proportion of extreme events is comparable with about 8 dry/wet years each in 45 yr of observations and about 31 of each in 200 yr of model time. Like the observed, the precipitation over the southern part of New Zealand is more or less uniform throughout the year, varying between 90 and 110 mm month^{-1} (Fig. 8c). As also seen in the observed, there is a noticeable seasonal cycle in the North Island precipitation data (Fig. 8d), with mean peak rates of up to 120 mm month^{-1} during austral winter, declining steadily to a low-rainfall season of only 75–90 mm month^{-1} for austral summer. The seasonal cycle in North Island rainfall might be enhanced in the model because of the previously mentioned bias in the ITCZ and an excessively strong SPCZ, which is most promi-

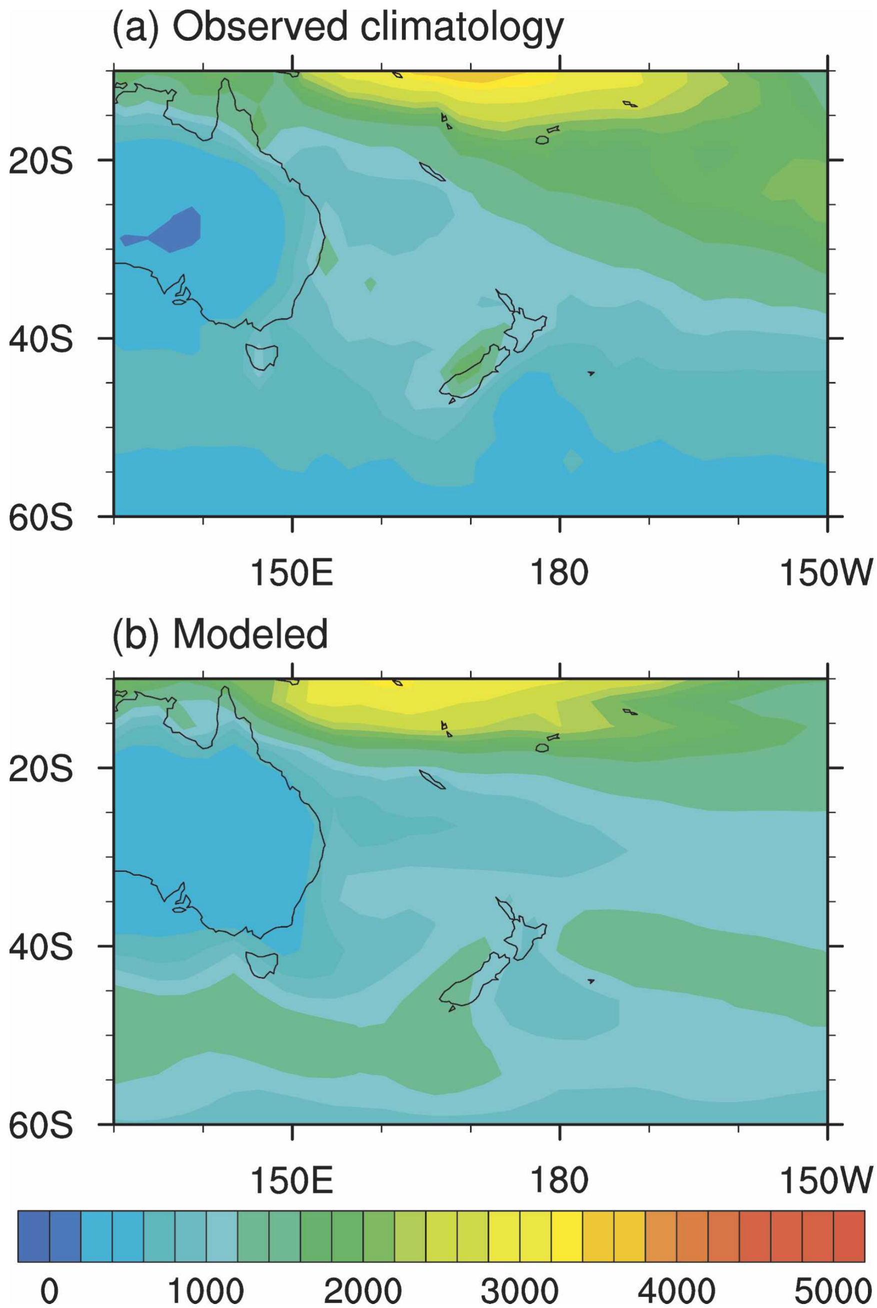

Fig. 7. Annual mean precipitation for (a) the CMAP climatology for the period 1979–2004 and (b) the model (both in mm yr^{-1}).

nent during June–August (Hack et al. 2006; Zhang and Wang 2006), when the observed SPCZ normally weakens (Collins et al. 2006). However, as is generally accepted, New Zealand rainfall occurs essentially uniformly throughout the year (Garnier 1958), with neither the model nor observed seasonality being statistically significant at the 90% confidence level. Spectral analysis (Figs. 8e,f) also indicates a difference in dominant frequencies for the two regions: for the South Island, peaks occur at approximately 4.3 and 2 yr, while the North Island shows a significant peak at approximately 2.9 yr, which happens to be in the range of the frequency associated with ENSO in the model (e.g., Kiehl and Gent 2004; Collins et al. 2006). Overall, considering the coarse resolution of the coupled climate model and the very localized nature of New Zealand precipitation,

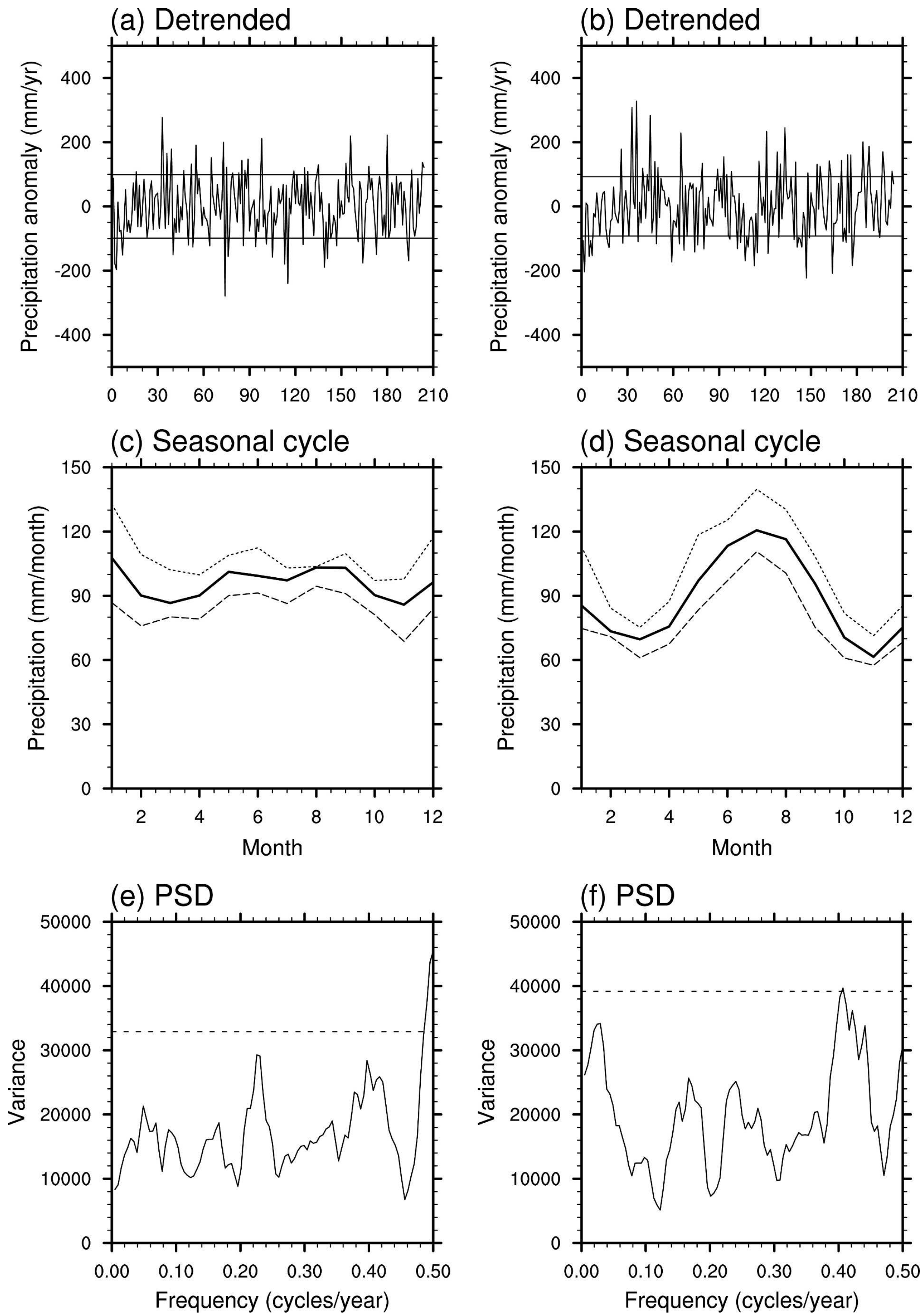

FIG. 8. Characteristics of model precipitation time series for the (left) South Island and (right) North Island: (a), (b) annual anomalies in mm yr^{-1} with horizontal lines indicating cutoff values for extreme years; (c), (d) seasonal cycle (mm $month^{-1}$) averaged over all years (solid line) or only dry (dashed) and wet (dotted) years, respectively; and (e), (f) power spectral density with theoretical white noise spectrum at the 90% confidence level (dashed horizontal line).

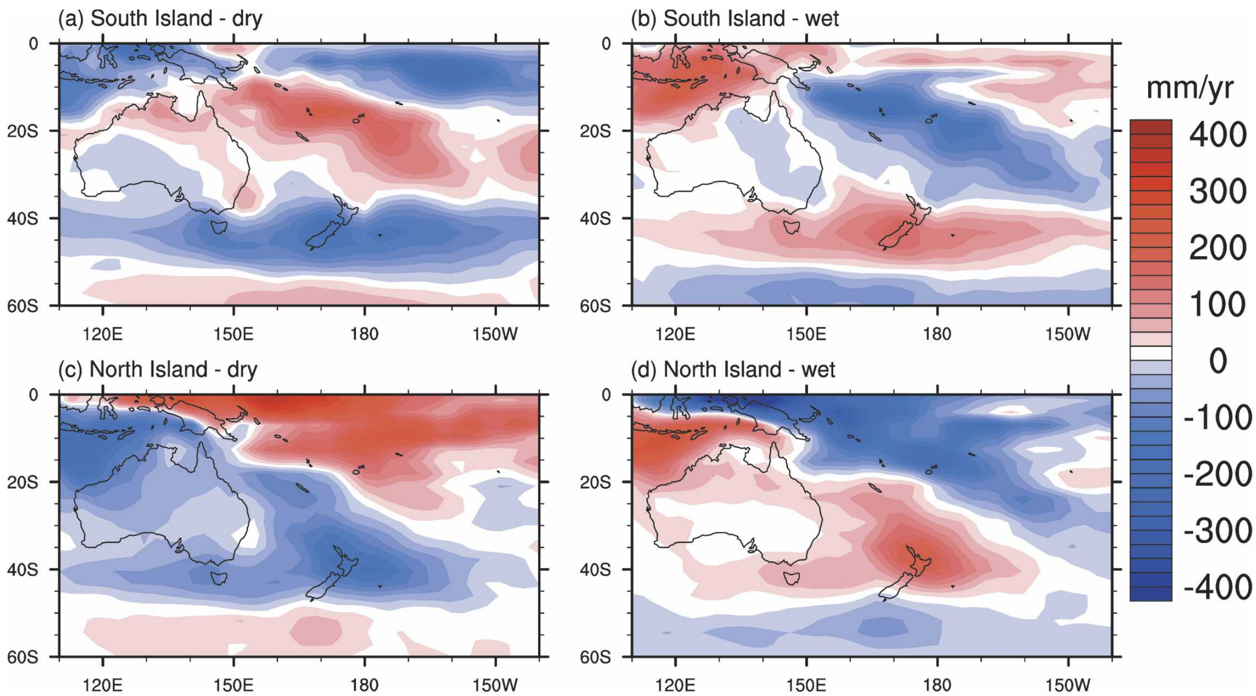

FIG. 9. Composites of model precipitation anomalies for (a), (b) South Island and (c), (d) North Island for anomalously (left) dry and (right) wet rainfall years. Color shaded regions indicate significant anomalies, while white areas are not significant at the 90% confidence level as estimated by a two-tailed t test.

the model represents the overall regional rainfall characteristics surprisingly well (Figs. 7 and 8).

The spatial distribution of significant precipitation anomalies during dry and wet South and North Island years in the model shows considerable large-scale features centered over the respective islands (Fig. 9). Naturally, the model's coarse grid cannot resolve the rich orography of each island, so our comparison is focused on large spatial scales, where they agree broadly with the observations (refer to Fig. 3). Dry (wet) South Island years are characterized by below (above) normal rainfall (in excess of 200 mm yr^{-1}) across the country, with the exception of the very northern coast of the North Island experiencing wet (dry) conditions (Figs. 9a,b). This out-of-phase relationship of the north coast rainfall with the remaining country during South Island dry years is encountered in the observations as well, though over a slightly larger area (Fig. 3a). For North Island anomalous rainfall years, a clear latitudinal gradation in rainfall anomalies is seen, with southern regions of the South Island experiencing progressively smaller anomalies (Figs. 9c,d). Again, the very southern tip of the South Island shows out-of-phase rainfall anomalies with the rest of the country, reminiscent of the observations (Figs. 3c,d). Meridional gradients in rainfall anomalies for New Zealand extreme years are well represented in the model, while it does not capture observed zonal features because of the inability to resolve the rich orography of the north–south oriented mountain ranges across New Zealand.

Composites of anomalies of a range of variables in the model during years of anomalous precipitation are shown in Figs. 10, 11, and 12. During dry (wet) years for the South and North Island, an intensification (weakening) of the meridional SLP gradient is observed (Figs. 10a,b and 11a,b). However, the SLP anomalies for the North Island are weaker (only up to ± 1 hPa) and more localized in nature, concentrated over the Australian–New Zealand region, while those for the South Island are stronger (in excess of ± 1.5 hPa) and truly circumpolar. This agrees well with the observed composite SLP patterns described above, although overall the model composite fields appear more zonal. The SLP composites for both the North and South Island are reminiscent of the pattern of SLP anomaly associated with the SAM (Hall and Visbeck 2002; Sen Gupta and England 2006), though more so for the case of the South Island. The intensified (weakened) SLP gradient during dry (wet) South and North Island years leads to increased (decreased) westerlies south of 45°S and more easterly (westerly) anomalies for the latitude band 20°–40°S (Figs. 10c,d and 11c,d). For the South Island, the anomalies in the westerlies (in excess of ± 0.8 m s^{-1}) are again circumpolar, while the zonal

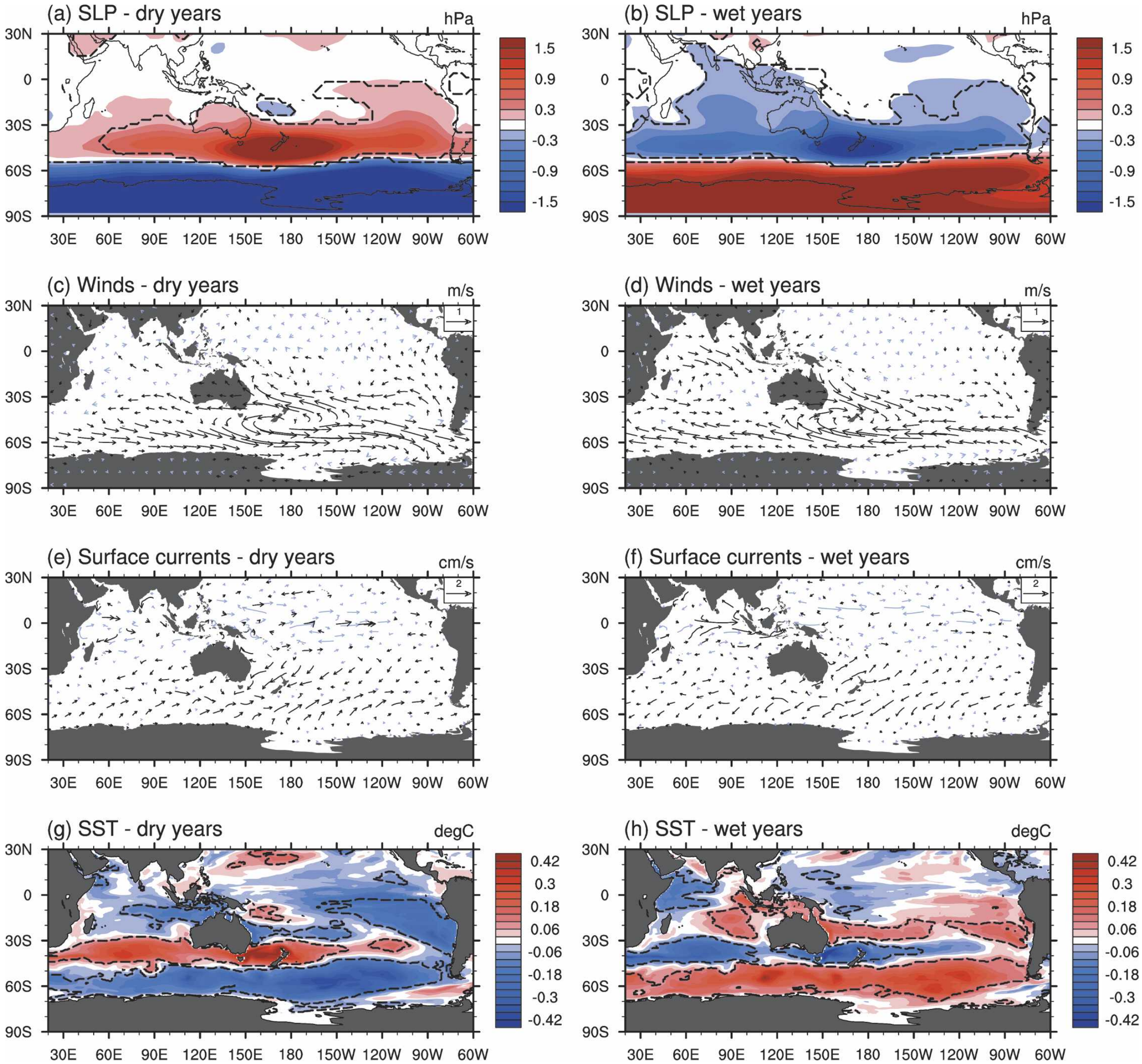

FIG. 10. Composite anomalies in model (a), (b) SLP, (c), (d) winds, (e), (f) surface currents, and (g), (h) SST for the South Island for anomalously (left) dry and (right) wet rainfall years. Dashed lines and black vectors indicate significant anomalies at the 90% confidence level as estimated by a two-tailed *t* test.

wind anomalies in the subtropics are less extensive. The North Island zonal wind anomalies are weaker and focus on the Australian–New Zealand region, especially during wet years over northern New Zealand. The meridional winds show more northerly (southerly) anomalies to the south of Australia and across southern New Zealand for dry (wet) South and North Island years, and southerly (northerly) wind anomalies over northern New Zealand and to the northeast of Australia (Figs. 10c,d and 11c,d). The meridional wind anomalies for the South Island are again stronger (up to ±0.5 m s^{-1}) and more extensive than the corresponding anomalies for the North Island (only up to ±0.3 m s^{-1}). Both zonal and meridional wind anomalies essentially follow the SLP distribution according to geostrophy.

Composites of anomalous surface ocean velocity fields (Figs. 10e,f and 11e,f) depict ocean currents responding to the changed wind fields via Ekman transport and geostrophic adjustment. During dry (wet) South and North Island years, significantly enhanced (weakened) northeastward zonal currents occur south of 45°S, agreeing well with the intensification (weakening) of the westerlies. The anomalies in surface zonal current velocity for anomalously dry and wet years over

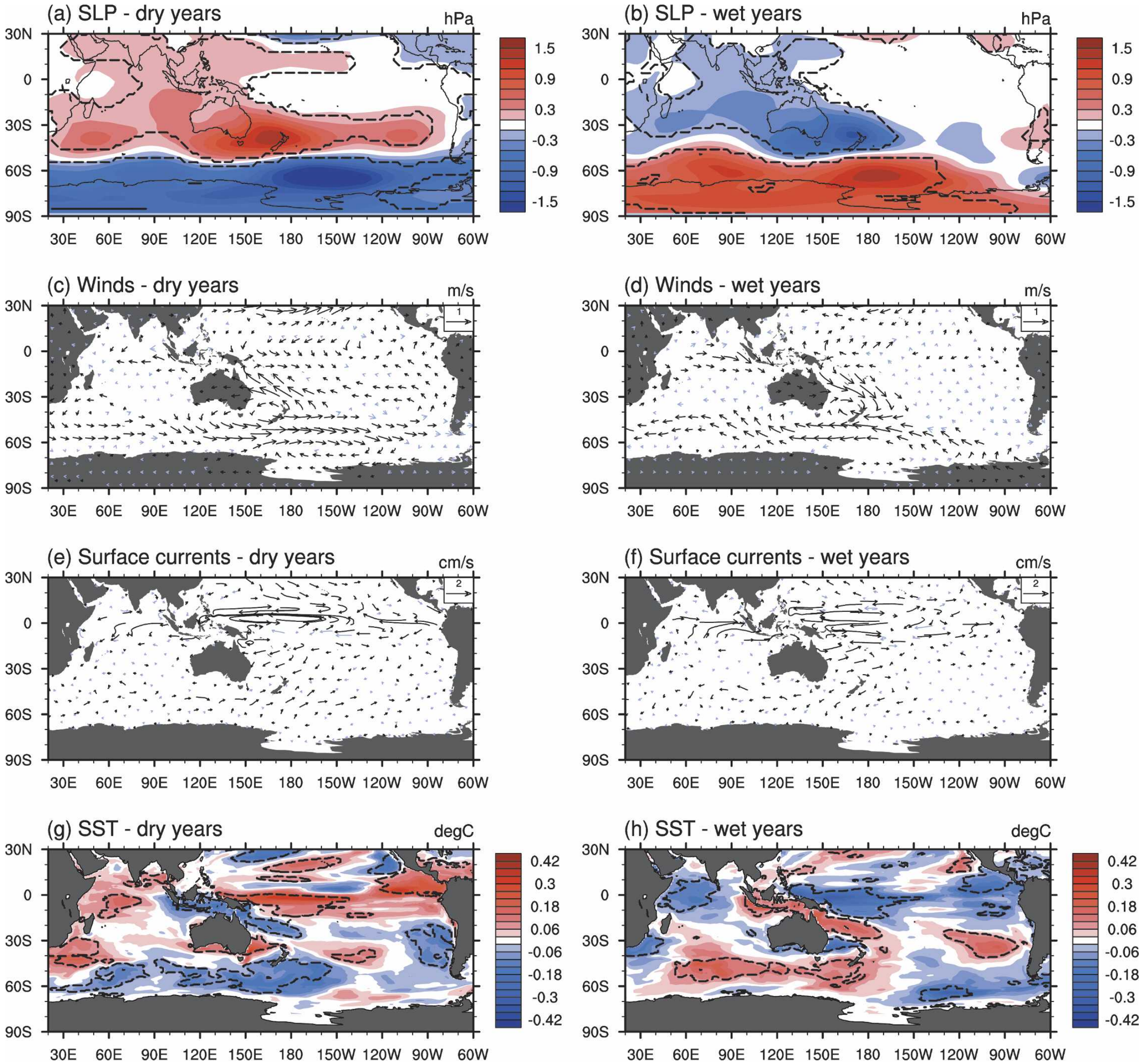

FIG. 11. Same as Fig. 10, but for North Island.

the South Island are circumpolar in extent and stronger (in excess of ± 2 cm s^{-1}) than the weaker (only up to ± 1 cm s^{-1}) anomalies for northern New Zealand. Northern New Zealand dry and wet years show alternating bands of eastward and westward anomalies in surface currents in the western tropical Pacific Ocean that are missing in the case of southern New Zealand. The strong and significant current anomalies in the western equatorial Pacific suggest the role of tropical processes in North Island rainfall variability. In contrast, during South Island dry/wet years, strong ocean current anomalies in the latitude band 30°–60°S underlying the subpolar westerlies hint at a modulating effect in the extratropics.

SST anomalies are affected by the changed wind and current fields, with composites showing a band of cold (warm) SST for dry (wet) years for 50°–70°S (Figs. 10g,h and 11g,h). For South Island dry and wet years, this band of anomalous SST is in excess of ± 0.4°C and circumpolar in extent, while it is weaker (only up to ± 0.3°C) and more localized just to the south of New Zealand and Australia in the case of northern New Zealand anomalous rainfall years. Furthermore, a band of warm (cold) SST during dry (wet) years for 30°–45°S of similar magnitude (in excess of ± 0.4°C) is only seen for southern New Zealand years, being only marginally apparent in North Island years. The warm (cold) SST anomalies for the latitudes 30°–45°S are established by

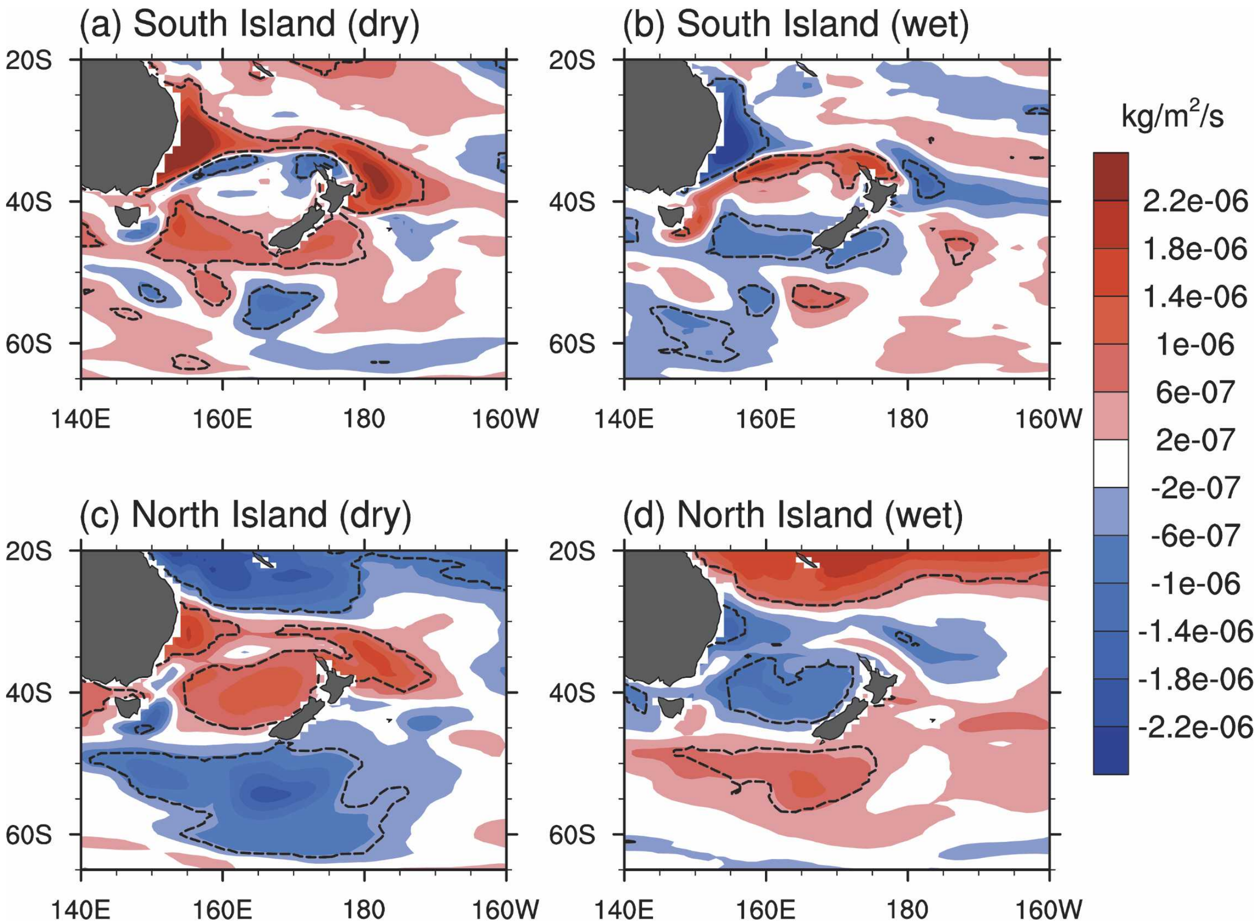

FIG. 12. Composite evaporation anomalies (in kg m^{-2} s^{-1}) in the model for the (a), (b) South Island and (c), (d) North Island for anomalously (left) dry and (right) wet rainfall years. Dashed lines indicate significant anomalies at the 90% confidence level as estimated by a two-tailed *t* test. Positive (negative) values indicate reduced (increased) evaporation out of the ocean.

anomalous Ekman transport due to the changed wind fields leading to a mass and heat convergence (divergence) at the interface of the easterly (westerly) to the north and westerly (easterly) zonal wind anomaly to the south. This is as would be expected during the positive (negative) phase of the SAM (e.g., Hall and Visbeck 2002; Sen Gupta and England 2006). This suggests a modulating influence of the SAM for the South Island anomalous rainfall years. In contrast, during North Island anomalous years, significant anomalies in SST occur in the tropical western equatorial Pacific Ocean, with the area 0°–10°S anomalously warm (cold) and the Coral Sea region unusually cold (warm) during dry (wet) years. This suggests ENSO plays a role in varying western Pacific SST anomalies and the regional atmospheric circulation via a northward displacement of the subpolar westerlies (Trenberth and Shea 1987) and changes to the SPCZ, which migrates eastward during El Niño years (Carleton 2003) and thus affects North Island rainfall. Almost no significant anomalies appear in the same areas for anomalously dry and wet years over the South Island, suggesting no direct influence of ENSO on that island's rainfall.

Anomalous surface air temperature (SAT; in excess of ±0.4°C; figure not shown) of warmer (cooler) anomalies over New Zealand occur during dry (wet) years over the South Island. Also apparent is anomalous cold (warm) SAT to the south of 45°S during dry (wet) years in southern New Zealand, most likely a result of underlying anomalous SST due to the strengthened (weakened) westerlies driving increased (decreased) anomalous northward Ekman transport (Fig. 10). The composites of anomalous SAT for North Island dry and wet years (figure not shown) indicate almost no significant anomalies across New Zealand, but cold (warm) anomalies to the south of the country, congruent with the SST anomalies (e.g., Mullan 1998) for dry (wet) North Island years. A stronger signal over the tropical Pacific, mirroring the underlying SST anomalies, can be seen in the western Pacific warm pool region (figure not shown), again suggestive of the greater importance of tropical processes in North as compared to South Island precipitation. The congruence of SAT to underlying SST contrasts findings by Basher and Thompson (1996), who suggested that both SAT and SST anomalies on interannual time scales are solely responses to the *meridional* wind component (i.e., southerly airflow resulting in colder temperatures), a result clearly not found in this study. Instead, we find that *zonal* wind anomalies and ensuing anomalous meridional Ekman transport contribute considerably to the SST anomaly, and in turn SAT patterns.

Composites of anomalies in relative humidity during South Island anomalous rainfall years (figures not shown) across New Zealand, the Tasman Sea, and southeast Australia show no consistent pattern of significant anomalies and do not vary in phase with the rainfall patterns (i.e., dry/wet year composites do not necessarily see drier/moister air over the adjacent oceans). In contrast, during dry (wet) North Island years, relative humidity is significantly decreased (increased) over the North Island of New Zealand and the surrounding ocean to the northwest of the island (figure not shown). Total cloud cover for dry (wet) South and North Island years is significantly reduced (increased) across all of New Zealand and the adjacent oceans (figures not shown). The composite anomalies in cloud cover during anomalous rainfall years in northern New Zealand vary in phase with those of tropical Australia, which is clearly not the case for those of the South Island.

To determine the respective role of the ocean anomalies in accounting for the rainfall anomalies over the two islands, anomalous surface heat flux (figures not shown) and evaporation (Fig. 12) composites are investigated. Emphasis is placed on evaporation anomalies, as evaporation most clearly differentiates the influence of oceanic versus atmospheric processes on rainfall. During dry (wet) South Island years, reduced (enhanced) evaporation anomalies appear in the Tasman Sea in a band extending from east of Tasmania across to the south of the South Island, and along the east coast of the South Island (Figs. 12a,b). This region of anomalous evaporation is at the interface of the westerly and easterly wind anomaly at 45°S, characterized by subsiding air masses and reduced cloud cover (figure not shown) during South Island dry years, while the situation is reversed during wet years. The location of anomalous evaporation for the South Island is hence determined directly by the wind anomalies and not by the SST anomaly pattern (cf. Figs. 12a,b to Figs. 10g,h). Since the evaporation anomalies do not mirror SST anomalies, we can confirm that the anomalous SST is only symptomatic of the changed wind field and resultant anomalous Ekman transport, as proposed earlier, and not a driving factor influencing South Island rainfall during dry and wet years. In contrast, evaporation composites for North Island dry (wet) years depict reduced (enhanced) evaporation to occur for much of the Tasman Sea, while anomalies of the reverse sign appear south of New Zealand between 50° and 60°S (Figs. 12c,d). This corresponds closely to the patterns of anomalous SST seen in Figs. 11g,h, with high (low) evaporation overlying anomalously warm (cool) SST. This demonstrates the role of local air–sea heat fluxes driven by anomalous SST on North Island precipitation anomalies.

4. Links to Southern Hemisphere climate modes

From the results presented thus far, there appears to be a higher influence of the tropical Pacific Ocean region on the North Island climate, while southern New Zealand seems to be mostly affected by the atmospheric circulation in the midlatitudes. The circumpolar character of the South Island anomalies, both in the reanalyses and the model, suggests a dominant role of the SAM. To evaluate this further we now analyze composites of New Zealand precipitation during El Niño and La Niña years and extreme years in the SAM during the recent observational record for 1960–2004 and in the 200-yr natural variability model run.

Composite anomalies of New Zealand precipitation during El Niño and La Niña years reveal very different influences by the respective ENSO phases (Fig. 13). During El Niño years, drier conditions occur for much of the North Island and the very northern edge of the South Island (Fig. 13a). The decrease in rainfall is significant in the northeast of the North Island with annual precipitation levels dropping by almost 400 mm yr^{-1}. The very southern and southwestern regions of the South Island experience moderately wetter conditions (up to 200 mm yr^{-1}), though only partially significant. The anomalous rainfall distribution during El Niño years (Fig. 13a) is very reminiscent of that of the North Island dry years (Fig. 3c), two of which were El Niño years (Table 1). Enhanced southwesterly airflow across the country during El Niño years (Fig. 13e; see also Waugh et al. 1997; Kidson and Renwick 2002), due to a northward displacement of the westerlies and higher incidence of cold fronts (Trenberth and Shea 1987), accounts for wetter southern and western regions while reducing rainfall further north. These southwesterly anomalies across the country resemble the anomalous winds seen during North Island dry years (Fig. 5c), as expected during times of below-average precipitation.

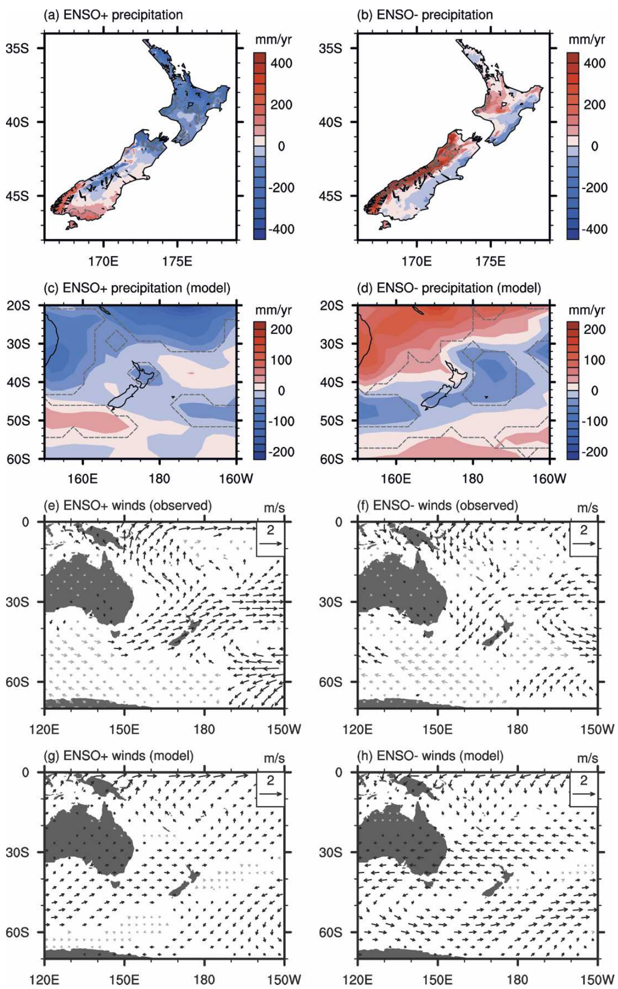

FIG. 13. Composite anomalies of annual (a), (b) observed and (c), (d) model New Zealand precipitation (in mm yr^{-1}) and (e), (f) NCEP and (g), (h) model winds (in m s^{-1}) during (left) El Niño and (right) La Niña years for the period 1960–2004. Dashed lines in (a)–(d) and black vectors in (e)–(h) indicate significant anomalies at the 90% confidence level as estimated by a two-tailed *t* test. Vector scale is indicated in (e)–(h) in m s^{-1} at top right of the diagram.

In contrast, during La Niña years, no significant anomalies appear for the North Island and eastern regions of the South Island, while along the entire west coast of the South Island significant above-average precipitation occurs (up to 400 mm yr^{-1} above normal; Fig. 13b). In turn, the rainfall anomalies during La Niña years (Fig. 13b) appear similar to South Island wet years (Fig. 3b), with two of the latter categorized as La Niña years (Table 1). The distribution of anomalous rainfall during La Niña years is caused by anomalous northerly winds (Fig. 13f; see also Waugh et al. 1997; Kidson and Renwick 2002), as already seen during wet North Island years (Fig. 5d), depositing increased moisture onto the mountainous west coast of the South Island and parts of the North Island. The respective anomalies in precipitation and circulation across the Southern Alps confirm those found by Fitzharris et al. (1997) for glacial mass balances for the shorter period 1977–93. Across the entire country, the precipitation changes during ENSO years agree in principle with those of Kidson and Renwick (2002) for the period 1979–2001, though they furthermore stratified their analysis by season and distinguished between moderate and strong El Niño years, which is beyond the scope of this study.

The model precipitation anomalies during El Niño years (Fig. 13c), though of smaller magnitude, agree well in their spatial distribution with the observed (Fig. 13a); that is, anomalous dry conditions occurred across New Zealand except over the southernmost tip of the South Island. The model winds during El Niño years (Fig. 13g) also show enhanced westerly flow across New Zealand, though their magnitude is only half of the observed. In contrast during La Niña years, the model does not capture the northerly flow anomalies across New Zealand (Fig. 13h), which explains the poor agreement between the observed and model precipitation anomalies, especially over the South Island (Figs. 13b,d). The poor representation of the situation during La Niña years in the model might be due in part to the simple method used to determine model La Niña years (i.e., as those below one standard deviation in the Niño-3.4 index).

The patterns of anomalous New Zealand precipitation and wind fields over the region during anomalous SAM years are presented in Fig. 14. It should be noted that the phase of the SAM not only indicates the location of the subpolar westerlies (and the associated moisture advection); it also acts as a proxy for the latitude of extratropical storm tracks (e.g., Fyfe 2003). During positive SAM years, much of New Zealand experiences drier than normal conditions, with the exception of the very northernmost edges of both islands, which see slightly enhanced rainfall by up to 200 mm yr^{-1} (Fig. 14a). The decrease in precipitation everywhere else in the country lies generally around 100–250 mm yr^{-1}, although in the high-rainfall region along the mountainous west coast of the South Island anomalies reach in excess of 400 mm yr^{-1}. However, considering the anomalies in terms of a variation coefficient of rainfall (not shown), the reduction in rainfall is of a similar order of magnitude across both islands.

The anomalous rainfall distribution during positive SAM years can be understood as a response to the changed wind fields with enhanced northeasterly flow over the country (Fig. 14e), supplying the northern edges of the two islands with increased rainfall, while

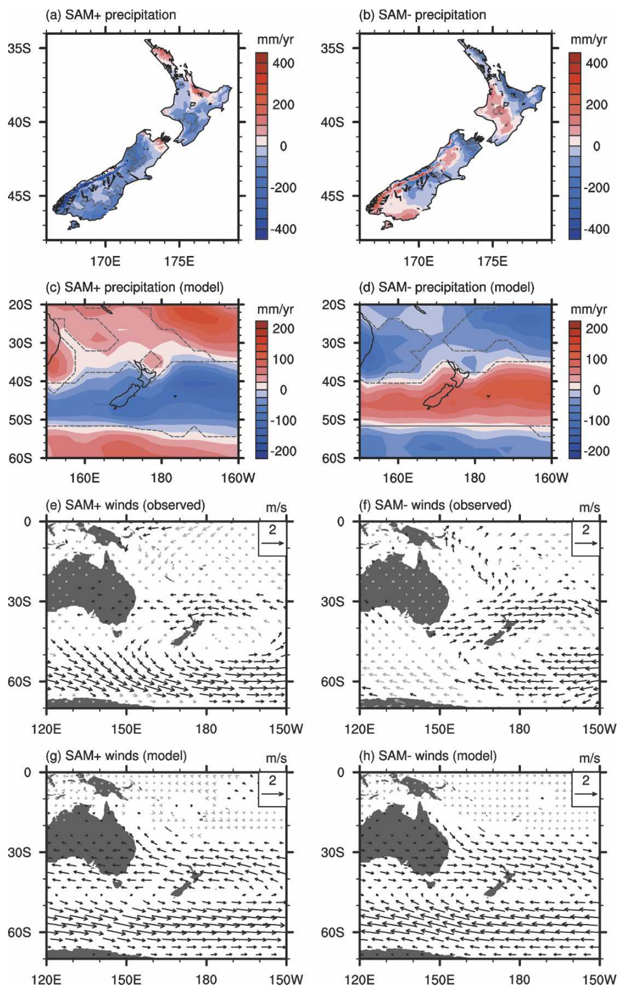

FIG. 14. Same as Fig. 13, but for (left) positive and (right) negative SAM years.

precipitation levels elsewhere are lowered. The anomalous wind field agrees with the circulation changes described by Hall and Visbeck (2002) during the high-index phase of the SAM and is similar to those seen for South Island dry years in this study (Fig. 4c). The distribution of anomalous rainfall during the positive SAM phase is very similar to the situation evident during anomalously dry South Island years (Fig. 3a), of which two are positive SAM years (Table 1). It is reversed during negative SAM years, with increased rainfall in the Southern Alps, the southern tip of the South Island and much of the North Island (Fig. 14b). Again, the northernmost edges of the two islands are out of phase with the rest of the country, being anomalously dry with annual rainfall up to 300 mm yr^{-1} below average. While the rainfall distribution across the North Island closely approximates reversed conditions between the positive and negative phase of the SAM, the South Island shows more asymmetry between these extreme phases: during the positive SAM, the South Island experiences dry conditions everywhere (Fig. 14a). In contrast, for the negative SAM the South Island is characterized by greater heterogeneity and finescale structure in the precipitation anomalies (Fig. 14b). The anomalous westerly/southwesterly winds across the country (Fig. 14f) correspond with the described rainfall changes and are reminiscent of the changed wind field during South Island wet years (Fig. 4d). The anomalously low (high) rainfall along the west coast of the South Island during positive (negative) SAM years, with weakened (enhanced) westerlies and enhanced (weakened) northerly airflow, agree with the findings of Clare et al. (2002) for glacial mass balances in the Southern Alps. The above analyses were repeated with a monthly time series for the SAM, giving robust results, as would be expected given the short time scale for the atmosphere to respond to the annular mode.

The situation during model SAM years agrees very well with observations during the positive phase: dry conditions occur across the country except along the very northern coast of the North Island (Fig. 14c) and easterly flow anomalies dominate (Fig. 14g), as seen during South Island dry years (Fig. 10c), though they extend further south in the model compared to the observations (Fig. 14e). The model precipitation and wind anomalies during the negative SAM phase (Figs. 14d,h) are mirror images of the positive phase. However, the observations show more local intra-island variation in rainfall (Fig. 14b), especially over the South Island, which is not resolved by the model because of the finescale orography of that island.

The ENSO in the model has a spectral peak of 2–3 yr (e.g., Kiehl and Gent 2004; Collins et al. 2006), a frequency also dominant for the North Island rainfall time series in the model (Fig. 8f). However, the composites do not show as strong a signal in the SST anomalies in the equatorial Pacific Ocean in the model (Fig. 11) as they do in the observed (Fig. 5). Figures 6c,d show that the amplitude of ENSO in the model is lower compared to the observed, which may account for the weaker SST signature in the composites.

The difference in seasonal cycle between the two islands (Figs. 2e,f and 8e,f) can also be understood as a result of the predominant influence of different phenomena for each region; namely tropical/subtropical influences and ENSO for the North Island and the high-latitude SAM for the South Island rainfall. The axis of the subtropical high-pressure belt migrates from around 26°S in winter to around 36°S in summer (Mosley and Pearson 1997) and associated with this anticyclonic conditions dominate during summer over the

North Island, accounting for reduced rainfall then (Figs. 2f and 8f). North Island seasonal precipitation is modulated by ENSO, with the largest ENSO-related changes occurring in austral winter (Kidson and Renwick 2002), the high-rainfall season in the North Island. This essentially keeps the seasonal rainfall distribution during anomalous North Island years more or less equivalent to average years (Figs. 2f and 8f). In contrast, the South Island on average displays uniform rainfall distribution throughout the year (Figs. 2e and 8e), as is typical of a midlatitude climate dominated by the influence of the subpolar westerlies. However, during dry and wet South Island precipitation years, the deviation in rainfall from the average seasonal distribution occurs predominantly during austral spring (and to a lesser degree also for autumn; Fig. 2e), the most active season of the SAM (Thompson and Wallace 2000). The fact that the model does not show this strong deviation from the average seasonal cycle during anomalously dry and wet years (Fig. 8e) could be attributed to a weak seasonal cycle in the SAM in the NCAR CCSM2 model (Alex Sen Gupta 2006, personal communication). An investigation of seasonal rainfall variations in response to the SAM is beyond the scope of this study, although this has been undertaken already for ENSO (e.g., Kidson and Renwick 2002).

5. Summary and conclusions

We have assessed interannual and multidecadal variability in New Zealand rainfall, both in observations and a global coupled climate model. Variability in precipitation across New Zealand was shown to be predominantly modulated by two Southern Hemisphere climate modes, namely ENSO and the SAM, with a latitudinal gradation in influence of the respective phenomena.

1) For the North Island, local air–sea heat fluxes and circulation changes associated with the tropical ENSO mode play an important role. North Island anomalously dry (wet) years are characterized by locally increased (reduced) SLP, cold (warm) SST anomalies in the southern Tasman Sea and to the north of the island, and a coinciding reduced (enhanced) evaporation upstream of the southwesterly (northeasterly) airflow.
2) South Island precipitation variability is dominated by the strength and position of the subpolar westerlies, which are modulated by the extratropical SAM. During anomalously dry (wet) years in precipitation for southern New Zealand, an enhanced (reduced) meridional SLP gradient occurs, with circumpolar strengthened (weakened) subpolar westerlies and an easterly (westerly) anomaly in zonal wind north of that. Cold (warm) SST anomalies appear underlying the subpolar westerlies, while anomalies of the opposite sign occur further north around New Zealand. The easterly (westerly) zonal wind anomaly across the island lead to decreased (increased) moisture transport onto the island. White and Cherry (1999) describe similar anomalies in SST and meridional winds that are associated with above and below-average rainfall for New Zealand, associating these anomalies with the ACW. In contrast, we find clear circumpolar anomalies in this study, especially for the South Island, suggesting a dominant influence of the SAM for southern New Zealand rainfall.
3) During El Niño years, drier conditions are apparent for the entire North Island and the northern edge of the South Island, while enhanced precipitation occurs on the southwestern edge of the South Island, because of enhanced southwesterly airflow across the country. The anomalous rainfall distribution during El Niño years is very reminiscent of that of the North Island dry years.
4) In contrast, La Niña leads to increased rainfall solely along the mountainous west coast of the South Island, due to anomalous northerly airflow depositing heightened moisture onto the mountains. The rainfall anomalies during La Niña years appear similar to South Island wet years.
5) During the positive (negative) phase of the SAM, via changes to the general atmospheric circulation, reduced (increased) precipitation occurs over much of the South Island and the southern regions of the North Island, while the northern edges of both islands are out of phase with these changes. The distribution of anomalous rainfall during the positive SAM phase is very similar to the situation in anomalously dry South Island years.

As stated previously, the results we have obtained were then reassessed with the recent CCSM3 model and the ERA-40 reanalysis fields, and our conclusions were found to be consistent.

The SAM has previously been linked to precipitation variability in midlatitudes; for example in South America (Silvestri and Vera 2003) and South Africa (Reason and Rouault 2005). Thus, it is of little surprise to find rainfall over New Zealand, especially across the South Island, which is located in the subpolar westerly wind belt, also modulated by the SAM. Projections of a further trend toward the positive phase of the SAM under enhanced greenhouse forcing (Fyfe et al. 1999; Kushner et al. 2001), coupled with the previously described links between the SAM and New Zealand rainfall, suggest future patterns of New Zealand precipitation will be characterized by substantial anomalies from the long-term mean. This issue of recent trends in New Zealand precipitation will be investigated in more detail in a separate study.

Acknowledgments. We thank the National Institute of Water and Atmospheric Research in New Zealand for providing the precipitation dataset used in this study. Use of the CCSM2 and CCSM3 model output from the National Center for Atmospheric Research and their reanalysis dataset, jointly developed with the National Centers for Environmental Prediction and provided by NOAA/OAR/ESRL PSD, Boulder, Colorado, through their Web site (http://www.cdc.noaa.gov) is gratefully acknowledged. The CMAP Precipitation and NOAA-ERSST-V2 SST data was also provided by NOAA/OAR/ESRL PSD, Boulder, Colorado, and the ERA-40 data by the ECMWF. We would also like to thank Agus Santoso for help with the spectral analysis and three anonymous reviewers for their constructive comments. CCU was supported by the University of New South Wales under a University International Postgraduate Award, and MHE was supported by the Australian Research Council and a CSIRO Wealth from Oceans Fellowship.

REFERENCES

Basher, R. E., and C. S. Thompson, 1996: Relationship of air temperatures in New Zealand to regional anomalies in sea-surface temperature and atmospheric circulation. *Int. J. Climatol.,* **16,** 405–425.

Boville, B. A., and P. R. Gent, 1998: The NCAR Climate System Model, version one. *J. Climate,* **11,** 1115–1130.

Brahmananda Rao, V. B., A. M. C. do Carmo, and S. H. Franchito, 2003: Interannual variations of storm tracks in the Southern Hemisphere and their connections with the Antarctic Oscillation. *Int. J. Climatol.,* **23,** 1537–1545.

Cai, W., G. Shi, and Y. Li, 2005: Multidecadal fluctuations of winter rainfall over southwest western Australia simulated in the CSIRO Mark 3 coupled model. *Geophys. Res. Lett.,* **32,** L12701, doi:10.1029/2005GL022712.

Carleton, A. M., 2003: Atmospheric teleconnections involving the Southern Ocean. *J. Geophys. Res.,* **108,** 8080, doi:10.1029/2000JC000379.

Clare, G. R., B. B. Fitzharris, T. J. H. Chinn, and M. J. Salinger, 2002: Interannual variation in end-of-summer snowlines of the Southern Alps of New Zealand, and relationships with Southern Hemisphere atmospheric circulation and sea surface temperature patterns. *Int. J. Climatol.,* **22,** 107–120.

Collins, W. D., and Coauthors, 2006: The Community Climate System Model version 3 (CCSM3). *J. Climate,* **19,** 2122–2143.

England, M. H., C. C. Ummenhofer, and A. Santoso, 2006: Interannual rainfall extremes over southwest Western Australia linked to Indian Ocean climate variability. *J. Climate,* **19,** 1948–1969.

Fitzharris, B. B., T. J. Chinn, and G. N. Lamont, 1997: Glacier balance fluctuations and atmospheric circulation patterns over the Southern Alps, New Zealand. *Int. J. Climatol.,* **17,** 745–763.

Fyfe, J. C., 2003: Extratropical Southern Hemisphere cyclones: Harbingers of climate change? *J. Climate,* **16,** 2802–2805.

——, G. J. Boer, and G. M. Flato, 1999: The Arctic and Antarctic Oscillations and their projected changes under global warming. *Geophys. Res. Lett.,* **26,** 1601–1604.

Garnier, B. J., 1958: Climatic characteristics. *The Climate of New Zealand,* B. J. Garnier, Ed., Edward Arnold Publishers, 14–33.

Gong, D., and S. Wang, 1999: Definition of Antarctic Oscillation index. *Geophys. Res. Lett.,* **26,** 459–462.

Hack, J. J., J. M. Caron, S. M. Yeager, K. W. Oleson, M. M. Holland, J. E. Truesdale, and P. J. Rasch, 2006: Simulation of the global hydrological cycle in the CCSM Community Atmosphere Model version 3 (CAM3): Mean features. *J. Climate,* **19,** 2199–2221.

Hall, A., and M. Visbeck, 2002: Synchronous variability in the Southern Hemisphere atmosphere, sea ice, and ocean resulting from the annular mode. *J. Climate,* **15,** 3043–3057.

Hines, K. M., D. H. Bromwich, and G. J. Marshall, 2000: Artificial surface pressure trends in the NCEP–NCAR reanalysis over the Southern Ocean and Antarctica. *J. Climate,* **13,** 3940–3952.

Jones, J. M., and M. Widmann, 2003: Instrument- and tree-ring-based estimates of the Antarctic Oscillation. *J. Climate,* **16,** 3511–3524.

Kalnay, E., and Coauthors, 1996: The NCEP/NCAR 40-Year Reanalysis Project. *Bull. Amer. Meteor. Soc.,* **77,** 437–471.

Keable, M., I. Simmonds, and K. Keay, 2002: Distribution and temporal variability of 500 hPa cyclone characteristics in the Southern Hemisphere. *Int. J. Climatol.,* **22,** 131–150.

Kidson, J. W., and J. A. Renwick, 2002: Patterns of convection in the tropical Pacific and their influence on New Zealand weather. *Int. J. Climatol.,* **22,** 151–174.

Kiehl, J. T., and P. R. Gent, 2004: The Community Climate System Model, version 2. *J. Climate,* **17,** 3666–3682.

Kistler, R., and Coauthors, 2001: The NCEP–NCAR 50-Year Reanalysis: Monthly means CD-ROM and documentation. *Bull. Amer. Meteor. Soc.,* **82,** 247–267.

Kushner, P. J., I. M. Held, and T. L. Delworth, 2001: Southern Hemisphere atmospheric circulation response to global warming. *J. Climate,* **14,** 2238–2249.

Madden, R. A., D. J. Shea, R. W. Katz, and J. W. Kidson, 1999: The potential long-range predictability of precipitation over New Zealand. *Int. J. Climatol.,* **19,** 405–421.

Marshall, G. J., 2002: Trends in Antarctic geopotential height and temperature: A comparison between radiosonde and NCEP–NCAR reanalysis data. *J. Climate,* **15,** 659–674.

——, 2003: Trends in the Southern Annular Mode from observations and reanalyses. *J. Climate,* **16,** 4134–4143.

——, and S. A. Harangozo, 2000: An appraisal of NCEP/NCAR reanalysis MSLP data viability for climate studies in the South Pacific. *Geophys. Res. Lett.,* **27,** 3057–3060.

Meehl, G. A., P. R. Gent, J. M. Arblaster, B. L. Otto-Bliesner, E. C. Brady, and A. Craig, 2001: Factors that affect the amplitude of El Niño in global coupled climate models. *Climate Dyn.,* **17,** 515–526.

Meneghini, B., I. Simmonds, and I. N. Smith, 2006: Association between seasonal Australian rainfall and the Southern Annular Mode. *Proc. Eighth Int. Conf. on Southern Hemisphere*

Meteorology and Oceanography, Foz do Iguacu, Brazil, INPE, 311–313.

Meyers, G., P. McIntosh, L. Pigot, and M. Pook, 2007: The years of El Niño, La Niña, and interactions with the tropical Indian Ocean. *J. Climate,* **20,** 2872–2880.

Mosley, M. P., and C. P. Pearson, 1997: Hydrological extremes and climate in New Zealand. *Floods and Droughts: The New Zealand Experience,* M. P. Mosley and C. P. Pearson, Eds., New Zealand Hydrological Society, 1–14.

Mullan, A. B., 1998: Southern Hemisphere sea-surface temperatures and their contemporary and lag association with New Zealand temperature and precipitation. *Int. J. Climatol.,* **18,** 817–840.

Reason, C. J. C., and M. Rouault, 2005: Links between the Antarctic Oscillation and winter rainfall over western South Africa. *Geophys. Res. Lett.,* **32,** L07705, doi:10.1029/2005GL022419.

Renwick, J. A., 2004: Trends in the Southern Hemisphere polar vortex in NCEP and ECMWF reanalyses. *Geophys. Res. Lett.,* **31,** L07209, doi:10.1029/2003GL019302.

——, J. J. Katzfey, K. C. Nguyen, and J. L. McGregor, 1998: Regional model simulations of New Zealand climate. *J. Geophys. Res.,* **103,** 5973–5982.

Salinger, M. J., and A. B. Mullan, 1999: New Zealand climate: Temperature and precipitation variations and their links with atmospheric circulation 1930–1994. *Int. J. Climatol.,* **19,** 1049–1071.

——, and G. M. Griffiths, 2001: Trends in New Zealand daily temperature and rainfall extremes. *Int. J. Climatol.,* **21,** 1437–1452.

——, R. E. Basher, B. B. Fitzharris, J. E. Hay, P. D. Jones, J. P. Macveigh, and I. Schmidely-Leleu, 1995: Climate trends in the Southwest Pacific. *Int. J. Climatol.,* **15,** 285–302.

——, J. A. Renwick, and A. B. Mullan, 2001: Interdecadal Pacific Oscillation and South Pacific climate. *Int. J. Climatol.,* **21,** 1705–1721.

Sen Gupta, A., and M. H. England, 2006: Coupled ocean–atmosphere–ice response to variations in the Southern Annular Mode. *J. Climate,* **19,** 4457–4486.

Silvestri, G. E., and C. S. Vera, 2003: Antarctic Oscillation signal on precipitation anomalies over southeastern South America. *Geophys. Res. Lett.,* **30,** 2115, doi:10.1029/2003GL018277.

Simmonds, I., and K. Keay, 2000: Mean Southern Hemisphere extratropical cyclone behavior in the 40-year NCEP–NCAR reanalysis. *J. Climate,* **13,** 873–885.

Smith, T. M., and R. W. Reynolds, 2003: Extended reconstruction of global sea surface temperatures based on COADS data (1854–1997). *J. Climate,* **16,** 1495–1510.

——, and ——, 2004: Improved extended reconstruction of SST (1854–1997). *J. Climate,* **17,** 2466–2477.

Thompson, D., and J. Wallace, 2000: Annular modes in the extratropical circulation. Part I: Month-to-month variability. *J. Climate,* **13,** 1000–1016.

Trenberth, K. E., and D. J. Shea, 1987: On the evolution of the Southern Oscillation. *Mon. Wea. Rev.,* **115,** 3078–3096.

Uppala, S. M., and Coauthors, 2005: The ERA-40 re-analysis. *Quart. J. Roy. Meteor. Soc.,* **131,** 2961–3012.

Waugh, J., H. Freestone, and D. Lew, 1997: Historic floods and droughts in New Zealand. *Floods and Droughts: The New Zealand Experience,* M. P. Mosley and C. P. Pearson, Eds., New Zealand Hydrological Society, 29–50.

White, W. B., and N. J. Cherry, 1999: Influence of the Antarctic circumpolar wave upon New Zealand temperature and precipitation during autumn–winter. *J. Climate,* **12,** 960–976.

Xie, P., and P. A. Arkin, 1996: Analyses of global monthly precipitation using gauge observations, satellite estimates, and numerical model predictions. *J. Climate,* **9,** 840–858.

Yin, J. H., 2005: A consistent poleward shift of the storm tracks in simulations of 21st century climate. *Geophys. Res. Lett.,* **32,** L18701, doi:10.1029/2005GL023684.

Zelle, H., G. J. van Oldenborgh, G. Burgers, and H. Dijkstra, 2005: El Niño and greenhouse warming: Results from ensemble simulations with the NCAR CCSM. *J. Climate,* **18,** 4669–4683.

Zhang, G., and H. Wang, 2006: Toward mitigating the double ITCZ problem in NCAR CCSM3. *Geophys. Res. Lett.,* **33,** L06709, doi:10.1029/2005GL025229.